arXiv:cond-mat/0301264v3 [cond-mat.mes-hall] 15 Jul 2003

Electronic Transport in Hybrid Mesoscopic Structures: A Nonequilibrium Green Function Approach

Zhao Yang Zeng,[1,2] Baowen Li,[1] and F. Claro[3]

[1] *Department of Physics, National University of Singapore, 117542, Singapore*
[2] *Department of Physics, Hunan Normal University, Changsha 410081, China*
[3] *Facultad de Física, Pontificia Universidad Católica de Chile, Casilla 306, Santiago 22, Chile*

(Dated: February 2, 2008)

We present a unified transport theory of hybrid structures, in which a confined normal state (N) sample is sandwiched between two leads each of which can be either a ferromagnet (F) or a superconductor (S) via tunnel barriers. By introducing a four-dimensional Nambu-spinor space, a general current formula is derived within the Keldysh nonequilibrium Green function formalism, which can be applied to various kinds of hybrid mesoscopic systems with strong correlations even in the nonequilibrium situation. Such a formula is gauge invariant. We also demonstrate analytically for some quantities, such as the difference between chemical potentials, superconductor order parameter phases and ferromagnetic magnetization orientations, that only their relative value appears explicitly in the current expression. When applied to specific structures, the formula becomes of the Meir-Wingreen-type favoring strong correlation effects, and reduces to the Landauer-Büttiker-type in noninteracting systems such as the double-barrier resonant structures, which we study in detail beyond the wide-band approximation. We find that the spin-dependent density of states of the ferromagnetic lead(s) is reflected in the resonant peak and resonant shoulder structure of the I-V characteristics of $F/I/N/I/F$ structures with large level spacing. The tunnel magnetoresistance that exhibits complex behaviors as a function of the bias voltage, can be either positive or negative, suppressed or enhanced within the resonant peak region(s), depending on the couplings to the leads. The Andreev current spectrum of $F/I/N/I/S$ structures consists of a series of resonant peaks as a function of the gate voltage, of which the number and amplitude are strongly dependent on the bias voltage, degree of spin polarization of the ferromagnetic lead, energy gap of the superconducting lead, and the level configuration of the central region. In $S/I/N/I/S$ resonant structures with asymmetric superconducting energy gaps, the Josephson current through a single resonant level is slightly enhanced in contrast to the significant enhancement of the Josephson current in $S/N/S$ Junctions. The current-phase relation is relevant to the level position and the couplings to the superconducting leads.

PACS numbers: 72.10.Bg,72.25.-b,74.50+r,73.21.-b

I. INTRODUCTION

Electronic transport in mesoscopic systems or nanoscale structures has received extensive theoretical and experimental attention.[1] In mesoscopic systems the sample size is smaller than the phase coherent length, and electrons retain their phase when travelling through the sample. In the ballistic limit, i.e., when the dimensions of the sample are smaller than the mean free path, electrons can traverse the system without any scattering. In contrast to macroscopic systems, the conductance of mesoscopic systems is sample-specific, since electron wavefunctions are strongly dependent on the form of the boundary of the sample and the configuration of scatterers located within the sample.

To calculate the conductance of mesoscopic systems, one should first consider the wave nature of electrons. The classical Boltzmann transport equation[2] is obviously inappropriate, since the assumption that electrons can be viewed as classical particles does not hold at a mesoscopic scale due to the Heinsenberg uncertainty limitation. Linear-response theory[3] is restricted to the weak perturbation regime and apparently can not be applied to the nonlinear or nonequilibrium situation. Electronic transport through a mesoscopic medium is in effect a wave transmitting process of electrons, which can be associated with a scattering matrix. In measuring the conductance one always connects the sample to electron reservoirs through perfect leads.[4] In a two-terminal setup ($\mathcal{L}$=left, $\mathcal{R}$=right), the Landauer-Büttiker formula[5] states that the current $\mathcal{I}$ can be expressed as a convolution of the transmission probability $\mathcal{T}$ and the Fermi distribution function f_α ($\alpha = \mathcal{L}, \mathcal{R}$), i.e., $\mathcal{I} = \frac{2e}{h}\int \mathcal{T}(\epsilon)[f_{\mathcal{L}}(\epsilon) - f_{\mathcal{R}}(\epsilon)]d\epsilon$. The conductance $\mathcal{G}$ in the linear-response regime is $\mathcal{G} = \frac{2e^2}{h}\int \mathcal{T}(\epsilon)(-\frac{\partial f}{\partial \epsilon})d\epsilon$. Such a formulation seems more appealing since the transport properties are encoded in the corresponding transmission probability, which can be calculated by various methods.

The nonequilibrium Green function (NEGF) approach[6,7,8,9] has proven to be a powerful technique to investigate transport problems in the many-body systems and mesoscopic systems. The equation of motion for the NEGF $G^<$, the quantum Boltzmann equation (QBE),[6] serves a starting point for many transport calculations in the many-body problems,[7,8] where a four-variable distribution function is required to incorporate the quantum effect due to the uncertainty principle. The Keldysh formalism of the NEGF,[9,10] due to its integral form, becomes a popular method in the formulation, calculation and simulation of recent mesoscopic transport problems. Caroli at al. were the first to employ the Keldysh NEGF technique to study the tunneling problems of a biased (nonequilibrium) metal-insulator-metal junction.[11] Meir and Wingreen[12] in 1992 derived a useful formula for the current through an interacting region with normal leads and applied it to investigate the transport properties of a quantum dot in Kondo and fractional quantum Hall regimes. Later the Keldysh NEGF formalism was used to analyze the I-V characteristics of superconductor-superconductor point contacts and the transport problem in a quantum dot with superconductor leads in Nambu space.[13,14,15] By introducing Green functions in the spinor space, the Keldysh NEGF approach has been also employed to study a quantum dot connected to two ferromagnetic electrodes.[16] Therefore, incorporating both Nambu and spinor spaces is a convenient device in order to investigate transport problems in the presence of both superconductors and ferromagnets within the Keldysh NEGF formalism. It is the purpose of this work to present a unified theory of electronic transport through an interacting region connected to either bulk ferromagnetic or superconducting leads. In such a formalism, resonant transmission due to single particle interference, correlation effects arising from to strong electron-electron interactions, ferromagnetism and superconductivity proximity effect in the presence of ferromagnets and superconductors can be treated in a systematic way. We noticed that there exists a circuit theory for mesoscopic systems developed by Nazarov et al.[20] based on the kinetic equations of quasiclassical Green functions,[19] which provides an alternative way to investigate the transport properties of hybrid structures with arbitrary connections.[20] However, such a formalism is not favorable to the systems of strong correlation, and apparently inapplicable to the cases where the single particle interference effect (for example, in resonant-tunneling structures) is prominent since the dependence on the relative coordinate of the quasiclassical Green functions is integrated out.

Thanks to recent advances in nanofabrication and material growth technologies, several kinds of hybrid mesoscopic structures have been realized experimentally. These nanoscale structures include mesoscopic junctions such as normal-metal/superconductor[22] (N/S) and ferromagnet/superconductor[23] (F/S) contacts, superconductor/insulator/superconductor[24] ($S/I/S$) and superconductor/ferromagnet/superconductor[25] ($S/F/S$) junctions, and certain kinds of resonant structures such as superconductor/quantum-dot/superconductor[26] ($S-QD-S$), normal-metal/superconducting quantum-dot/normal-metal[27] ($N-SQD-N$), normal-metal/ferromagnetic-quantum-dot/normal-metal[28] ($N-FQD-N$) transistors. In a normal-metal/superconductor (N/S) junction, Andreev reflection[29,30] dominates the transport process at low bias voltages, in which an electron in the normal metal slightly above the chemical potential of the superconductor is reflected as a hole slightly below the chemical potential at the interface between the normal metal and superconductor with an electron pair moving into the superconductor, and vice versa. When two superconductor components are coupled together through an insulator or a normal metal, electron pairs can move coherently from one superconductor to the other, yielding a nonzero current even in the zero bias limit-the well known DC Josephson effect, and an oscillating current at finite bias-the AC Josephson effect.[31] The $S/N/S$ Josephson junction must be a mesoscopic system, with the length smaller than the phase coherent length of electrons in the normal region, to ensure electron (hole)'s coherent motion inside the normal part. Then a reflected electron (hole) can interfere constructively with itself, a process that produces a set of decoupled forward or backward 'Andreev energy levels' carrying positive or negative Josephson current.[32,33] An impurity inside the normal region couples the Andreev energy levels, and thus modifies the quasi-particle energy spectrum and other quantities. In the presence of a ferromagnetic metal, a spin-polarized current may be induced due to the imbalance of the spin populations at the chemical potential.[34] Spin imbalance also introduces a net magnetic moment-the magnetization of ferromagnets. When two ferromagnets participate in a transport experiment, the relative orientation of the magnetizations of these two ferromagnets will play an important role in the transport properties, and the spin-valve effect arises.[35] Combining ferromagnets and superconductors, one may expect some new transport features, since there is no complete Andreev reflection at the F/S interface. The conductance of a F/S junction can be either smaller or larger than the N/S case, depending on the degree of spin polarization of the ferromagnet.[36] When ferromagnets, superconductors and confined (interacting) normal metals are integrated together, the interplay between ferromagnetism, superconductivity and electron-electron interaction is anticipated to lead to more interesting and more complicated transport properties. Despite the basic interest in the fundamental theory as mentioned above, hybrid mesoscopic systems also boast potential applications in future electronic devices which employ both the charge and spin degree of freedom of electrons.

Starting from a microscopic Hamiltonian, we derive in this paper a general current formula within the Keldysh NEGF formalism for hybrid mesoscopic systems in which a central nanoscale interacting normal region is weakly connected to two leads, each of which is either a ferromagnet or a superconductor, thus providing a unified theory of electron transport in general hybrid structures, which incorporates resonant tunneling, strong correlation, ferromagnetism and superconductivity proximity effect. Such a formula can be also applied to the nonequilibrium situation. Rather than from the original mean-field Stoner ferromagnet[36] and BCS superconductor Hamiltonian,[31] we calculate the current from their diagonalized forms after appropriate Bogoliubov transformations, with which the ferromagnetism and superconducting proximity as well as the chemical potentials of the system are embodied in the tunneling parts of the system Hamiltonian. Such a procedure is found to be a crucial step in the analysis of our transport problem, and facilitates the applications of the general formula to the specific forms for given structures, which are Meir-Wingreen-type formulae.[12] Employing such a procedure it is very easy to check whether such a theory satisfies the condition of gauge invariance, a requirement of all transport theories. Moreover, the energy-dependence and bias-voltage-dependence of the level-width functions and the distribution functions in the current formula are derived in a strict and natural way, while this has been done somewhat phenomenologically in the other formalisms.[9,12,15,16,17] This merit allows us to investigate the I-V characteristics of hybrid mesoscopic systems with a much more broad bias region. In addition we demonstrate that only their relative value for some physical quantities appears in the current formula after some unitary transformations. These quantities include the chemical potential, magnetization orientation of ferromagnet and the phase of the superconductor order parameter. Physically only their relative value can be measured in a transport experiment for these physical quantities, thus justifying the ad hoc assumption that one of them can be always set to zero.[13,14,15,16] Such a formalism can be directly extended to the cases with more than two external leads, which can be either ferromagnetic or superconducting. A shorter paper which summarizes the formulation has been reported elsewhere.[37]

In order to illustrate the validity and versatility of our formulation, we apply the derived formulae to a non-interacting double-barrier resonant structure (DBTS) beyond the wide-band approximation which is usually used in the Keldysh NEGF formalisms.[9,12,14,15,16] We neglect the interaction effects, since in a regime where these interactions are not important, we can then see more clearly how ferromagnetism and superconductivity influence the transport properties of a normal metal resonant structure coupled to ferromagnetic and/or superconducting leads. As demonstrated in Section III, we derive the final current formula based on our formulation in a more systematic and economic way than others.[15,17] Some unexpected and novel transport features are found. When the level spacing of the central normal region is comparable to the bandwidth of the ferromagnetic lead(s), the I-V curves show resonant peaks plus resonant shoulders, reflecting directly the profile of the density of states (DOS) of the Stoner ferromagnet. This observation provides an alternative way to measure the degree of spin polarization of the system. The tunnel magnetoresistance (TMR) decreases non monotonically, as well as oscillates, as a function of the applied bias voltage between the ferromagnetic leads. It is enhanced or suppressed within the resonant regions depending on the couplings to the two sides. We also find negative TMR at some bias voltages in the strong coupling limit. These features tell us that there is richer physics in the TMR of a resonant structure. In the presence of ferromagnetic and superconucting leads, a series of peaks emerges in the Andreev current whenever the resonant Andreev reflection condition at the N/S interface is satisfied as the gate voltage applied to the central part varies. The number and height of these Andreev current peaks are strongly dependent on the bias voltage and the degree of spin polarization of the ferromagnet lead. Interesting step and peak structures are observed in the I-V characteristics, which may be used to determine the DOS of both ferromagnetic and superconducting leads. Finally we investigate the DC Josephson current in $S/I/N/I/S$ structures. It is shown that the DC Josephson current is slightly enhanced if the energy gaps of superconductors becomes asymmetric, in contrast to the $S/N/S$ systems. The current-phase relation is also weakly dependent on the asymmetry of the superconductor energy gaps.

The rest of this paper is organized as follows: In Section II the full Hamiltonian of an interacting normal metal placed in between either ferromagnetic or superconducting bulk leads is given. We first express the current in terms of the nonequilibrium Green functions in the Nambu-spinor space in general cases, and then present current expressions for the specific structures. The gauge invariance is proven to hold as well. Section III is devoted to the applications of the current formulae derived in Section II to non-interacting double-barrier structures, with a detailed analysis based on the analytical results and numerical demonstrations. Concluding remarks are given in Section IV. An appendix is included to present the expressions of the self-energy matrices and level-width matrices due to the elastic couplings to the leads.

II. FORMULATION OF THE PROBLEM

We consider electron motion along the longitudinal direction x in a hybrid sandwich structure schematically shown in Fig. 1. The central part is assumed to be in the normal state, connected via tunnel barriers (insulators or point contacts, etc.) to two bulk materials acting as leads, each of which can be either a ferromagnet, or a conventional BCS superconductor. We adopt the Stoner model[36,38] for the ferromagnet and the BCS Hamiltonian[31] for the superconductor. The Stoner model Hamiltonian is characterized by a mean-field exchange magnetization $\mathbf{h}$, and can be written as

$$H^F = \int dx \Psi^\dagger(x)\Big(-\frac{\hbar^2}{2m^*}\nabla_x^2 - \hat{\sigma}\cdot\mathbf{h} - \mu\Big)\Psi(x), \qquad (1)$$

where m^* is the electron effective mass, $\hat{\sigma} = (\hat{\sigma}_x, \hat{\sigma}_y, \hat{\sigma}_z)$ is the Pauli spin operator, μ is the chemical potential

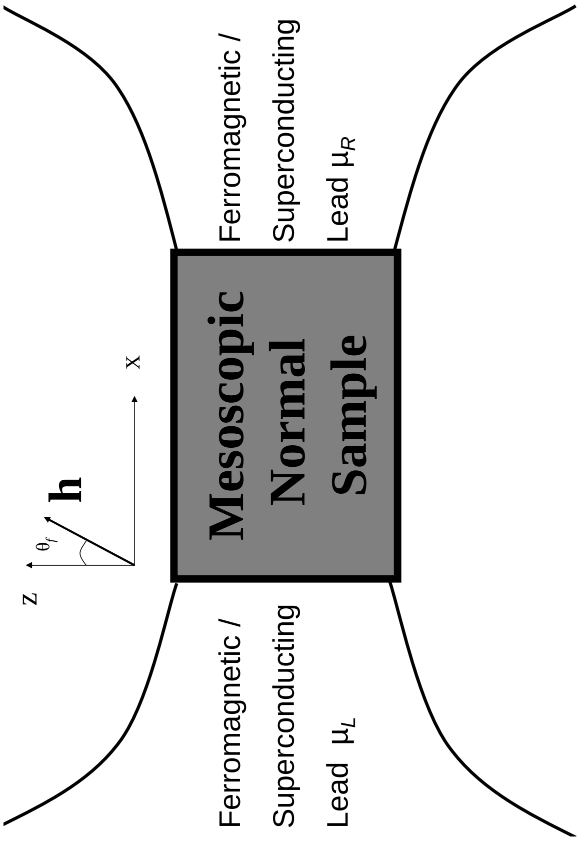

FIG. 1: A schematic diagram of a two-terminal hybrid mesoscopic structure. A mesoscopic normal region is attached to either ferromagnetic or superconducting leads with chemical potential $\mu_{\mathcal{L}}$ and $\mu_{\mathcal{R}}$. In the former case the magnetization **h** makes an angle θ_f relative to the normal z axis. The current is assumed to flow along the longitudinal x axis from the higher-chemical-potential lead to the lower-chemical-potential one.

and $\Psi^\dagger = (\psi_\uparrow^\dagger, \psi_\downarrow^\dagger)$ is the spinor field. In what follows we assume that the magnetization **h** makes an angle θ_f relative to the z axis, while we ignore the orientation with respect to the plane perpendicular to the transport direction being not relevant to the transport properties.[38]

Within the mean-field approximation, the BCS Hamiltonian takes the form

$$H^S = \sum_\sigma \int dx \Psi_\sigma^\dagger(x)\Big(-\frac{\hbar^2}{2m^*}\nabla_x^2 - \mu\Big)\Psi_\sigma(x) + \int dx\big[\Delta(x)\Psi_\uparrow^\dagger(x)\Psi_\downarrow^\dagger(x) - \Delta^*(x)\Psi_\downarrow(x)\Psi_\uparrow(x)\big]. \quad (2)$$

In Eq. (2) Ψ_σ is the field operator of electrons with spin $\sigma =\uparrow,\downarrow$, $\Delta(x) = U\langle\Psi_\uparrow(x)\Psi_\downarrow(x)\rangle$ is the off-diagonal pair potential, with U a negative constant characterizing the electron-electron attraction. In general the pair potential Δ needs to be determined self-consistently, and in this work will be assumed to be position and energy independent for simplicity.

Since we are concerning about transport properties of electrons rather than their motion in real space it is more convenient to deal with the lead Hamiltonian in k-space. Expanding the electron field operator in terms of the eigenfunctions of the momentum operator in the longitudinal(tunneling) direction as $\Psi_\sigma(x) = \sum f_{k\sigma}e^{ikx}(s_{k\sigma}e^{ikx})$ we cast the ferromagnet and superconductor Hamiltonian (1) and (2) into the following forms in k-space (subscript $\gamma = \mathcal{L}$ and $\mathcal{R}$ are added to denote which side of the structure the ferromagnet or superconductor is located at)

$$\begin{aligned}\mathcal{H}_\gamma^{(F)} &= \sum_{k\sigma}[\varepsilon_{\gamma k} - sgn(\sigma)h_\gamma\cos\theta_{\gamma f} - \mu_\gamma]f_{\gamma k\sigma}^\dagger f_{\gamma k\sigma} \\ &\quad + \sum_{k\sigma} h_\gamma \sin\theta_{\gamma f} f_{\gamma k\sigma}^\dagger f_{\gamma k\bar{\sigma}}, \quad (3)\\ \mathcal{H}_\gamma^{(S)} &= \sum_{k\sigma}(\varepsilon_{\gamma k} - \mu_\gamma)s_{\gamma k\sigma}^\dagger s_{\gamma k\sigma} + \\ &\quad \sum_k \Big[\Delta_\gamma s_{\gamma k\uparrow}^\dagger s_{\gamma -k\downarrow}^\dagger + \Delta_\gamma^* s_{\gamma -k\downarrow} s_{\gamma k\uparrow}\Big], \quad (4)\end{aligned}$$

where $\varepsilon_{\gamma k} = \hbar^2 k^2/2m^*$, $\bar{\sigma}$ stands for the opposite to σ. Here the order parameter Δ_γ is characterized by its magnitude and phase: $|\Delta_\gamma|e^{i\varphi_\gamma}$, and, as we will show, $|\Delta_\gamma|$ opens an energy gap in the excitation spectrum of the superconductor. $f_{\gamma k\sigma}(f_{\gamma k\sigma}^\dagger)$ and $s_{\gamma k\sigma}(s_{\gamma k\sigma}^\dagger)$ are the electron destruction (creation) operators of spin σ in state k in the ferromagnet and superconductor, respectively. Henceforth, the notations $\sigma =\uparrow,\downarrow$ and $\sigma = \pm$ are used interchangeably. In what follows physical quantities such as the particle operator ψ, particle energy ε, and the chemical potential μ of the different parts are labelled by subscript $\gamma = \mathcal{L}, \mathcal{R}; \mathcal{C}$, whenever convenient. In addition, ferromagnetic or superconducting characteristics of the leads is stressed by adding a subscript or a superscript f or s to some quantities.

The Hamiltonian of the central region $\mathcal{H}_\mathcal{C}$ in momentum space can be modeled by

$$\mathcal{H}_\mathcal{C} = \sum_{n\sigma}(\varepsilon_{n\sigma} - \mu_\mathcal{C})\psi_{cn\sigma}^\dagger\psi_{cn\sigma} + \mathcal{H}_{int}(\{\psi_{cn\sigma}^\dagger\},\{\psi_{cn\sigma}\}), \quad (5)$$

where $\psi_{cn\sigma}^\dagger(\psi_{cn\sigma})$ creates (destroys) an electron of spin σ in state n, and $\mathcal{H}_{int}$ represents the interaction terms in the central region. It may include the electron-electron Coulomb interaction

$$\mathcal{H}_{int}^{el-el} = \sum_{\substack{n,m,\sigma,\sigma' \\ n\sigma \neq m\sigma'}} U_{n\sigma,m\sigma'}\psi_{cn\sigma}^\dagger\psi_{cn\sigma}\psi_{cm\sigma'}^\dagger\psi_{cm\sigma'}, \quad (6)$$

or the electron-phonon interaction

$$\mathcal{H}_{int}^{el-ph} = \sum_q \hbar\omega_q\zeta_q^\dagger\zeta_q + \sum_{n,\sigma;q} U_{n\sigma,q}\psi_{cn\sigma}^\dagger\psi_{cn\sigma}(\zeta_q^\dagger + \zeta_{-q}). \quad (7)$$

Here the first term is the free-phonon Hamiltonian, while the second represents the electron-phonon interaction, with interaction matrix element $U_{n\sigma,q}$. $\zeta_q^\dagger(\zeta_q)$ is the phonon creation (destruction) operator in mode q.

The couplings between the leads and the central region can be modeled by tunneling Hamiltonian, no matter how the leads are coupled to the central region, provided the couplings are not strong enough. Certainly the coupling strengths depend on the detailed configuration of the setup and should be determined in a self-consistent manner. However, for simplicity they are assumed known and can be written as

$$\begin{aligned}\mathcal{H}_T^{\gamma(F)} &= \sum_{kn;\sigma}\left[V_{kn;\sigma}^{\gamma f} f_{\gamma k\sigma}^\dagger \psi_{cn\sigma} + V_{kn;\sigma}^{\gamma f*}\psi_{cn\sigma}^\dagger f_{\gamma k\sigma}\right], \quad (8)\\ \mathcal{H}_T^{\gamma(S)} &= \sum_{kn;\sigma}\left[V_{kn;\sigma}^{\gamma s} s_{\gamma k\sigma}^\dagger \psi_{cn\sigma} + V_{kn;\sigma}^{\gamma s*}\psi_{cn\sigma}^\dagger s_{\gamma k\sigma}\right]. \quad (9)\end{aligned}$$

To see tunneling processes more clearly, and, more importantly, to facilitate the analysis of gauge invariance and the simplification of the general current formula (31) to the forms of specific systems, we first diagonalize the Hamiltonian of the leads by Bogoliubov transformations. For the ferromagnetic lead one has

$$f_{\gamma k\sigma} = \cos(\theta_{\gamma f}/2)\psi_{\gamma f k\sigma} - sgn(\sigma)\sin(\theta_{\gamma f}/2)\psi_{\gamma f k\bar{\sigma}}, \tag{10}$$

and for the superconducting lead,

$$e^{-i\varphi_\gamma/2}s_{\gamma k\sigma} = \cos\theta_{\gamma sk}\psi_{\gamma sk\sigma} + sgn(\sigma)\sin\theta_{\gamma sk}\mathcal{P}\psi_{\gamma sk\bar{\sigma}}^\dagger. \tag{11}$$

In Eqs. (10,11), $\mathcal{P}^\dagger(\mathcal{P})$ is the pair creation (destruction) operator guaranteeing particle conservation, which transforms a given N-particle state into an (N+2)-particle ((N-2)-particle) state, i.e., $\mathcal{P}^\dagger/\mathcal{P}|N\rangle = |N+2\rangle/|N-2\rangle$, and

$$\theta_{\gamma sk} = \arctan\left(\frac{\varepsilon_{\gamma k} + \sqrt{\varepsilon_{\gamma k}^2 + |\Delta_\gamma|^2}}{\varepsilon_{\gamma k} - \sqrt{\varepsilon_{\gamma k}^2 + |\Delta_\gamma|^2}}\right)^{1/2}. \tag{12}$$

Substituting the Bogoliubov transformations (10) and (11) into the lead Hamiltonian (3) and (4), we get the following diagonalized forms for the ferromagnetic and superconducting leads, respectively,

$$\begin{aligned}\mathcal{H}_\gamma^{(F)} &= \sum_{k\sigma}[\varepsilon_{\gamma k} - sgn(\sigma)h_\gamma - \mu_\gamma]\psi_{\gamma f k\sigma}^\dagger\psi_{\gamma f k\sigma}\\ &= \sum_{k\sigma}\varepsilon_{\gamma f k\sigma}\psi_{\gamma f k\sigma}^\dagger\psi_{\gamma f k\sigma}, \quad (13)\\ \mathcal{H}_\gamma^{(S)} &= \sum_{k\sigma}(\sqrt{\varepsilon_{\gamma k}^2 + |\Delta_\gamma|^2} - \mu_\gamma)\psi_{\gamma sk\sigma}^\dagger\psi_{\gamma sk\sigma} +\\ &\qquad Constant\\ &= \sum_{k\sigma}\varepsilon_{\gamma sk}\psi_{\gamma sk\sigma}^\dagger\psi_{\gamma sk\sigma} + Constant \quad (14)\end{aligned}$$

Now the particle number operator commutes with the corresponding lead Hamiltonian. After the Bogoliubov transformations, the diagonalized lead Hamiltonian describe the excitation (quasi particle) properties. The minimum energy of the excitations in a superconductor is $|\Delta_\gamma|$, implying an energy gap in the excitation spectrum.

With the Bogoliubov transformations (10) and (11) we turn the tunneling Hamiltonian into

$$\begin{aligned}\mathcal{H}_T^{\gamma(F)} &= \sum_{kn;\sigma}\Big(V_{kn;\sigma}^{\gamma f}\big[\cos(\theta_{\gamma f}/2)\psi_{\gamma f k\sigma}^\dagger - sgn(\sigma)\sin(\theta_{\gamma f}/2)\psi_{\gamma f k\bar{\sigma}}^\dagger\big]\psi_{cn\sigma} +\\ &\qquad V_{kn;\sigma}^{\gamma f*}\psi_{cn\sigma}^\dagger\big[\cos(\theta_{\gamma f}/2)\psi_{\gamma f k\sigma} - sgn(\sigma)\sin(\theta_{\gamma f}/2)\psi_{\gamma f k\bar{\sigma}}\big]\Big), \quad (15)\\ \mathcal{H}_T^{\gamma(S)} &= \sum_{kn;\sigma}\Big(V_{kn;\sigma}^{\gamma s}\big[\cos\theta_{\gamma sk}\psi_{\gamma sk\sigma}^\dagger + sgn(\sigma)\sin\theta_{\gamma sk}\psi_{\gamma sk\bar{\sigma}}\mathcal{P}^\dagger\big]e^{i\varphi_\gamma/2}\psi_{cn\sigma} +\\ &\qquad V_{kn;\sigma}^{\gamma s*}\psi_{cn\sigma}^\dagger e^{-i\varphi_\gamma/2}\big[\cos\theta_{\gamma sk}\psi_{\gamma sk\sigma} + sgn(\sigma)\sin(\theta_{\gamma sk})\mathcal{P}\psi_{\gamma sk\bar{\sigma}}^\dagger\big]\Big). \quad (16)\end{aligned}$$

The associated physical processes are more obvious and clear in the semiconductor model:[31,40] an electron of spin σ in the central regime can tunnel into either the spin σ band or $\bar{\sigma}$ band of the ferromagnetic lead, or tunnel into a spin σ state or condensate into an electron pair with a hole state of opposite spin being created, and vice versa.

In superconductors, correlation between two creation or annihilation quasi-particle operators with opposite spins are very important, relating to the Andreev reflection in transport processes. When ferromagnets are introduced, the correlation between a creation and an annihilation quasi-particle operator with opposite spins needs to be considered. To incorporate these two kinds of correlations in a unified way and consider the ferromagnet and superconductor on the same footing, we here introduce a generalized Nambu-spin representation spanning a 4-dimensional spin-orientated particle-hole space $\boldsymbol{\Psi}_x = \left(\psi^\dagger_{x\uparrow} \quad \psi_{x\downarrow} \quad \psi^\dagger_{x\downarrow} \quad \psi_{x\uparrow}\right)^\dagger$. Within the Keldysh NEGF formalism, Green functions are defined as

$$\mathbf{G}_{x,y}(t_1,t_2) = i\langle T_C[\boldsymbol{\Psi}_x(t_1)\otimes\boldsymbol{\Psi}^\dagger_y(t_2)]\rangle, \qquad (17)$$

where T_C is the time-ordering operator along the closed time path.[9] The usual retarded/advanced and lesser/greater Green functions then take the form

$$\begin{aligned}
\mathbf{G}^{r/a}_{\alpha,\beta}(t_1,t_2) &= \sum_{i,j}\mathbf{G}^{r/a}_{\alpha i,\beta j}(t_1,t_2) \\
&= \mp i\vartheta(\pm t_1 \mp t_2)\sum_{i,j}\langle[\boldsymbol{\Psi}_{\alpha i}(t_1)\otimes \\
&\qquad \boldsymbol{\Psi}^\dagger_{\beta j}(t_2) + \boldsymbol{\Psi}^\dagger_{\beta j}(t_2)\otimes\boldsymbol{\Psi}_{\alpha i}(t_1)]\rangle, \\
\mathbf{G}^{</>}_{\alpha,\beta}(t_1,t_2) &= \sum_{i,j}\mathbf{G}^{</>}_{\alpha i,\beta j}(t_1,t_2) \\
&= \pm i\sum_{i,j}\langle\boldsymbol{\Psi}^\dagger_{\beta j}(t_2)/\boldsymbol{\Psi}_{\alpha i}(t_1)\otimes \\
&\qquad \boldsymbol{\Psi}_{\alpha i}(t_1)/\boldsymbol{\Psi}^\dagger_{\beta j}(t_2)\rangle,
\end{aligned}$$

where $\alpha,\beta = \gamma f, \gamma s, c$ and $i,j = k,n$.

In this 4-dimensional Nambu-spinor space the total Hamiltonian can be rewritten in the following compact form

$$\mathcal{H} = \mathcal{H}_{\mathcal{C}} + \mathcal{H}_{\mathcal{L}} + \mathcal{H}_{\mathcal{R}} + \mathcal{H}^{\mathcal{L}}_{\mathcal{T}} + \mathcal{H}^{\mathcal{R}}_{\mathcal{T}}, \qquad (18)$$

where

$$\begin{aligned}
\mathcal{H}_{\mathcal{C}} &= \sum_n \boldsymbol{\Psi}^\dagger_{cn}\mathbf{E}_{cn}\boldsymbol{\Psi}_{cn} + \\
&\qquad \mathcal{H}_{int}(\{\boldsymbol{\Psi}^\dagger_{cn},\boldsymbol{\Psi}_{cn}\}), \qquad (19) \\
\mathcal{H}^{(F/S)}_{\gamma} &= \sum_k \boldsymbol{\Psi}^\dagger_{\gamma f/sk}\mathbf{E}_{\gamma f/sk}\boldsymbol{\Psi}_{\gamma f/sk}, \qquad (20) \\
\mathcal{H}^{\gamma(F/S)}_{\mathcal{T}} &= \sum_{kn}\left[\boldsymbol{\Psi}^\dagger_{\gamma f/sk}\mathbf{V}^{\gamma f/s}_{kn}(t)\boldsymbol{\Psi}_{cn} + H.c.\right]. \qquad (21)
\end{aligned}$$

In writing down Eq. (19,20,21), we have introduced the energy matrices

$$\mathbf{E}_\alpha = \begin{pmatrix} \epsilon_{\alpha\uparrow} & 0 & 0 & 0 \\ 0 & -\epsilon_{\alpha\downarrow} & 0 & 0 \\ 0 & 0 & \epsilon_{\alpha\downarrow} & 0 \\ 0 & 0 & 0 & -\epsilon_{\alpha\uparrow} \end{pmatrix}, \qquad \alpha = cn, \gamma f/sk \qquad (22)$$

and the tunneling matrices

$$\begin{aligned}
\mathbf{V}^{\gamma f}_{kn}(t) &= \mathbf{R}^f(\frac{\theta_{\gamma f}}{2})\mathbf{V}^{\gamma f}_{kn}\mathbf{P}(\mu_{\gamma\mathcal{C}}t), \qquad (23) \\
\mathbf{V}^{\gamma s}_{kn}(t) &= \mathbf{R}^s(\theta_{\gamma sk})\mathbf{V}^{\gamma s}_{kn}\mathbf{P}(\mu_{\gamma\mathcal{C}}t + \frac{\varphi_\gamma}{2}), \qquad (24) \\
\mu_{\gamma\mathcal{C}} &= \mu_\gamma - \mu_{\mathcal{C}}
\end{aligned}$$

in which

$$\begin{aligned}
\mathbf{V}^{\gamma f/s}_{kn} &= \begin{pmatrix} V^{\gamma f/s}_{kn} & 0 & 0 & 0 \\ 0 & -V^{\gamma f/s*}_{kn} & 0 & 0 \\ 0 & 0 & V^{\gamma f/s}_{kn} & 0 \\ 0 & 0 & 0 & -V^{\gamma f/s*}_{kn} \end{pmatrix}, \\
\mathbf{R}^f(x) &= \begin{pmatrix} \cos x & 0 & \sin x & 0 \\ 0 & \cos x & 0 & -\sin x \\ -\sin x & 0 & \cos x & 0 \\ 0 & \sin x & 0 & \cos x \end{pmatrix}, \\
\mathbf{R}^s(x) &= \begin{pmatrix} \cos x & -\mathcal{P}\sin x & 0 & 0 \\ \mathcal{P}^*\sin x & \cos x & 0 & 0 \\ 0 & 0 & \cos x & \mathcal{P}\sin x \\ 0 & 0 & -\mathcal{P}^*\sin x & \cos x \end{pmatrix}, \\
\mathbf{P}(x) &= \begin{pmatrix} e^{ix/\hbar} & 0 & 0 & 0 \\ 0 & e^{-ix/\hbar} & 0 & 0 \\ 0 & 0 & e^{ix/\hbar} & 0 \\ 0 & 0 & 0 & e^{-ix/\hbar} \end{pmatrix}.
\end{aligned}$$

are the *coupling, rotation* and *phase* matrices, respectively. Note that we have performed a gauge transformation[39] to get the above Hamiltonian. Chemical potential is now incorporated in the phase operator $\mathbf{P}(\mu_{\gamma\mathcal{C}}t)$ in the tunneling matrices Eqs.(23,24), which along with the *rotation* operators is very useful to demonstrate gauge invariance for our system as shown below.

The current flowing from lead $\gamma = \mathcal{L},\mathcal{R}$ to the central region can be defined as the rate of change of the electron number $N_\gamma = \sum_{k\sigma} f^\dagger_{\gamma k\sigma}f_{\gamma k\sigma}(s^\dagger_{\gamma k\sigma}s_{\gamma k\sigma}) = \sum_{k\sigma}\psi^\dagger_{\gamma fk\sigma}\psi_{\gamma fk\sigma}(\psi^\dagger_{\gamma sk\sigma}\psi_{\gamma sk\sigma})$ in the lead. Within the Keldysh NEGF formalism, the current is expressed as

$$\begin{aligned}
\mathcal{I}_\gamma(t) &= -e < \dot{N}_\gamma > = \frac{ie}{\hbar} < [N_\gamma, H_{\mathcal{T}}] > \\
&= -\frac{e}{\hbar}\sum_{i=1,3}\sum_{nk}\Big([\mathbf{G}^<_{cn,\gamma f/sk}(t,t)\mathbf{V}^{\gamma f/s}_{kn}(t) - \\
&\qquad \mathbf{V}^{\gamma f/s\dagger}_{kn}(t)\mathbf{G}^<_{\gamma f/sk,cn}(t,t)]\Big)_{ii} \\
&= \frac{2e}{\hbar}\sum^{i=1,3}_{nk}\mathrm{Re}\left\{\left(\mathbf{V}^{\gamma f/s\dagger}_{kn}(t)\mathbf{G}^<_{\gamma f/sk,cn}(t,t)\right)_{ii}\right\}.
\end{aligned} \qquad (25)$$

Since the Hamiltonian of lead γ is of the form $\psi^\dagger_{\gamma f/sk\sigma}\psi_{\gamma f/sk\sigma}$, the equations of motion for $\mathbf{G}^<_{\gamma f/sk,cn}$ along with the Langreth analytic continuation[41] yield the following Dyson equations

$$\begin{aligned}
\mathbf{G}^<_{\gamma f/sk,cn}(t,t') &= \sum_m\int dt_1\Big[\mathbf{g}^r_{\gamma f/sk,\gamma f/sk}(t,t_1)\mathbf{V}^{\gamma f/s}_{km}(t_1) \\
&\qquad \mathbf{G}^<_{cm,cn}(t_1,t') + \mathbf{g}^<_{\gamma f/sk,\gamma f/sk}(t,t_1) \\
&\qquad \mathbf{V}^{\gamma f/s}_{km}(t_1)\mathbf{G}^a_{cm,cn}(t_1,t')\Big], \qquad (26) \\
\mathbf{G}^<_{cn,\gamma f/sk}(t,t') &= \sum_m\int dt_1\Big[\mathbf{G}^<_{cn,cm}(t,t_1)\mathbf{V}^{\gamma f/s\dagger}_{km}(t_1)
\end{aligned}$$

$$\mathbf{g}^r_{\gamma f/sk,\gamma f/sk}(t_1,t')+\mathbf{G}^r_{cn,cm}(t,t_1)\\ \mathbf{V}^{\gamma f/s\dagger}_{km}(t_1)\mathbf{g}^<_{\gamma f/sk,\gamma f/sk}(t_1,t')\Big],\quad(27)$$

in which the unperturbed retarded/advanced Green function $\mathbf{g}^{r/a}_{\gamma f/s,\gamma f/s}$ of lead γ can be readily obtained from the Hamiltonian $(13,14)$ as diagonal matrices

$$\begin{aligned}\mathbf{g}^{r/a}_{\gamma f/sk,\gamma f/sk}(t,t') &= \mp i\vartheta(\pm t\mp t')\\ &\quad\begin{pmatrix} g^{\uparrow -}_{\gamma f/sk} & 0 & 0 & 0\\ 0 & g^{\downarrow +}_{\gamma f/sk} & 0 & 0\\ 0 & 0 & g^{\downarrow -}_{\gamma f/sk} & 0\\ 0 & 0 & 0 & g^{\uparrow +}_{\gamma f/sk}\end{pmatrix}, &(28)\\ g^{\sigma\mp}_{\gamma f/sk}(t,t') &= e^{\mp i\varepsilon_{\gamma f/sk\sigma}(t-t')/\hbar}, &(29)\end{aligned}$$

and the lesser(greater) Green functions are related to the retarded(advanced) Green functions by $\mathbf{g}^{</>}_{\gamma f/sk,\gamma f/sk}(t,t') = \big[\mathbf{f}_\gamma(\varepsilon_{\gamma f/sk}) - \frac{1}{2}\mathbf{1} \pm \frac{1}{2}\mathbf{1}\big]\big[\mathbf{g}^a_{\gamma f/sk,\gamma f/sk}(t,t') - \mathbf{g}^r_{\gamma f/sk,\gamma f/sk}(t,t')\big]$. The Fermi distribution matrix $\mathbf{f}_\gamma(\varepsilon_{\gamma f/sk})$ reads

$$\mathbf{f}_\gamma(\varepsilon_{\gamma f/sk}) = \\ \begin{pmatrix} f(\varepsilon_{\gamma f/sk\uparrow}) & 0 & 0 & 0\\ 0 & f(-\varepsilon_{\gamma f/sk\downarrow}) & 0 & 0\\ 0 & 0 & f(\varepsilon_{\gamma f/sk\downarrow}) & 0\\ 0 & 0 & 0 & f(-\varepsilon_{\gamma f/sk\uparrow})\end{pmatrix},$$

where $f(x)=(1+e^{x/k_BT})^{-1}$ and we have used the relation $f(-x)=1-f(x)$.

Substituting Eq. (26) into (25), we obtain

$$\begin{aligned}\mathcal{I}_\gamma(t) &= \frac{2e}{\hbar}\sum_{nm}^{i=1,3}\int_{-\infty}^{t}dt_1\mathrm{Re}\Big\{\Big(\mathbf{\Sigma}^r_{\gamma f/s;nm}(t,t_1)\\ &\quad\mathbf{G}^<_{cm,cn}(t_1,t)+\mathbf{\Sigma}^<_{\gamma f/s;nm}(t,t_1)\\ &\quad\mathbf{G}^a_{cm,cn}(t_1,t)\Big)_{ii}\Big\}, \quad(30)\end{aligned}$$

where

$$\begin{aligned}\mathbf{\Sigma}^{r,a,</>}_{\gamma f/s;nm}(t_1,t_2) &= \sum_k \mathbf{V}^{\gamma f/s\dagger}_{kn}(t_1)\\ &\quad\mathbf{g}^{r/a,</>}_{\gamma f/sk,\gamma f/sk}(t_1,t_2)\mathbf{V}^{\gamma f/s}_{km}(t_2)\end{aligned}$$

is the self-energy matrix (see Appendix A) arising from electron tunneling between the central region and lead γ.

For steady transport, no charge piles up in the central normal region. One then has $\mathcal{I}_\mathcal{L}(t) = -\mathcal{I}_\mathcal{R}(t)$.[12] After symmetrizing the current formula (30), we finally get by setting $\mathcal{I}(t) = [\mathcal{I}_\mathcal{L}(t) - \mathcal{I}_\mathcal{R}(t)]/2$

$$\begin{aligned}\mathcal{I}(t) &= \frac{e}{\hbar}\sum^{i=1,3}\int_{-\infty}^{t}dt_1\mathrm{ReTr}\Big\{\Big(\big[\mathbf{\Sigma}^r_{\mathcal{L}f/s}(t,t_1)-\\ &\quad\mathbf{\Sigma}^r_{\mathcal{R}f/s}(t,t_1)\big]\mathbf{G}^<_{c,c}(t_1,t)+\big[\mathbf{\Sigma}^<_{\mathcal{L}f/s}(t,t_1)-\\ &\quad\mathbf{\Sigma}^<_{\mathcal{R}f/s}(t,t_1)\big]\mathbf{G}^a_{c,c}(t_1,t)\Big)_{ii}\Big\}, \quad(31)\end{aligned}$$

where the trace is over the level indices of the central region. Eq. (31) along with the self-energy matrices given in Appendix A is the central result of this work. The current is expressed in terms of the local properties ($\mathbf{G}^{r/a}$) and the occupation ($\mathbf{G}^{</>}$) of the central interacting region and the equilibrium properties ($\mathbf{\Sigma}^{</>}$) of the leads. It is emphasized that the current is usually independent of time except the presence of two superconductor leads with nonzero bias voltage. Formula (31) can be employed to investigate both equilibrium and nonequilibrium electronic transport in various kinds of hybrid mesoscopic systems, including $F/I/N/I/F$, $F/I/N/I/S$, $F/I/N/I/N$, $S/I/N/I/S$, $S/I/N/I/N$, and $F-QD-F$, $F-QD-S$, $F-QD-N$, $S-QD-S$, $S-QD-N$ structures as well, in which arbitrary interactions are allowed in the central part of the structure.

It is not difficult to check that Eq. (31) is gauge invariant, i.e., the current $\mathcal{I}(t)$ remains unchanged under a global energy shift in the whole region. This can be achieved through a gauge transformation for the Hamiltonian of the system

$$\begin{aligned}\hat{f}(\epsilon_0 t) &= \exp\Big\{\frac{i}{\hbar}\epsilon_0 t\big(\sum_{n\sigma}\psi^\dagger_{cn\sigma}\psi_{cn\sigma}\\ &\quad+\sum_{\gamma=\mathcal{L},\mathcal{R};k\sigma}\psi^\dagger_{\gamma f/sk\sigma}\psi_{\gamma f/sk\sigma}\big)\Big\},\end{aligned}$$

where ϵ_0 is just the energy shift. Such a gauge transformation gives rise, in turn, to the *phase* transformations of all the terms in the right-hand side of Eq. (31)

$$\begin{aligned}\mathbf{\Sigma}^{r/<}_{\gamma f/s}(t,t_1) &\to \mathbf{P}(\varepsilon_0 t)\mathbf{\Sigma}^{r/<}_{\gamma f/s}(t,t_1)\mathbf{P}^\dagger(\varepsilon_0 t_1),\\ \mathbf{G}^{a/<}_{c,c}(t_1,t) &\to \mathbf{P}^\dagger(\varepsilon_0 t_1)\mathbf{G}^{a/<}_{c,c}(t_1,t)\mathbf{P}(\varepsilon_0 t).\end{aligned}$$

The above procedures, equivalent to applying a *phase* transformation to the current operator: $\mathbf{P}^\dagger(\varepsilon_0 t)\mathcal{I}(t)\mathbf{P}(\varepsilon_0 t)$, ensure that the current remains the same under such a transformation. Therefore, the current formula (31) is gauge invariant.

Now we check whether the current becomes zero if we take the zero bias limit $\mu_\mathcal{L}=\mu_\mathcal{R}=\mu_0$. We first perform a *phase* operation $\mathbf{P}(\mu_{0\mathcal{C}}t+\varphi_\mathcal{R}/2)$ corresponding to the gauge transformation $\hat{f}(\mu_{\mathcal{C}0}t)$, $\mu_{0\mathcal{C}}=\mu_0-\mu_\mathcal{C}$ to Eq.(31), obtaining

$$\begin{aligned}\mathcal{I}(t) &= -\frac{e}{\hbar}\sum^{i=1,3}\int\frac{d\varepsilon}{2\pi}\mathrm{ImTr}\Big\{\Big(\frac{1}{2}\big[\tilde{\mathbf{\Gamma}}^{\mathcal{L}f/s}_{/\varrho}(\varepsilon)-\mathbf{\Gamma}^{\mathcal{R}f/s}_{/\varrho}(\varepsilon)\big]\\ &\quad\widetilde{\mathbf{G}}^<_{c,c}(\varepsilon)-\big[\tilde{\mathbf{\Gamma}}^{\mathcal{L}f/s}_{/\varrho}(\varepsilon)\mathbf{f}_\mathcal{L}(\varepsilon)-\mathbf{\Gamma}^{\mathcal{R}f/s}_{/\varrho}(\varepsilon)\mathbf{f}_\mathcal{R}(\varepsilon)\big]\\ &\quad\widetilde{\mathbf{G}}^a_{c,c}(\varepsilon)\Big)_{ii}\Big\}, \quad(32)\end{aligned}$$

where

$$\begin{aligned}\tilde{\mathbf{\Gamma}}^{\mathcal{L}f/s}_{/\varrho}(\varepsilon) &= \mathbf{P}^\dagger(\frac{\varphi_s}{2})\mathbf{\Gamma}^{\mathcal{L}f/s}_{/\varrho}(\varepsilon)\mathbf{P}(\frac{\varphi_s}{2}),\\ \widetilde{\mathbf{G}}^{r,a/<}_{c,c}(\varepsilon) &= \int d(t-t')e^{i\varepsilon(t-t')/\hbar}\mathbf{P}(\mu_{0\mathcal{C}}t+\frac{\varphi_\mathcal{R}}{2})\\ &\quad\mathbf{G}^{r,a/<}_{c,c}(t,t')\mathbf{P}^\dagger(\mu_{0\mathcal{C}}t'+\frac{\varphi_\mathcal{R}}{2}),\end{aligned}$$

with $\varphi_s = \varphi_{\mathcal{L}} - \varphi_{\mathcal{R}}$. From the fluctuation-dissipation theorem $\widetilde{\mathbf{G}}^{</>}_{c,c} = [\mathbf{f}_{eq}(\varepsilon) - \frac{1}{2}\mathbf{1} \pm \frac{1}{2}\mathbf{1}](\widetilde{\mathbf{G}}^{a}_{c,c} - \widetilde{\mathbf{G}}^{r}_{c,c})$ ($\mathbf{f}_{\mathcal{L}} = \mathbf{f}_{\mathcal{R}} = \mathbf{f}_{eq}$), one can readily verify that the current is zero except in the presence of two superconductor leads with different superconducting order parameter phases. In this case, there still exists a DC Josephson current in the zero bias limit due to the coherent tunneling of *quasi-particle pairs*. This can be seen more clearly in the expressions of the current in the specific systems (33,34,35).

Up to now we have obtained the expression for the current in a general case in which each of the two leads can be either a ferromagnet or a superconductor. Next we apply this general result (31) to the specific structures we are interested in. We first consider the case in which two leads are ferromagnetic. Inserting the expressions of the self-energy matrices $\mathbf{\Sigma}_{\gamma f}(t_1, t_2)$ (Appendix A) into Eq.(31), we get the current in a $F/I/N/I/F$ or $F-QD-F$ structure after a *rotation* transformation and a *phase* transformation

$$\begin{aligned}\mathcal{I}_{fnf} \;=\; & \frac{ie}{2\hbar}\sum^{i=1,3}\int\frac{d\varepsilon}{2\pi}\mathrm{Tr}\Big\{\Big(\big[\hat{\mathbf{\Gamma}}^{\mathcal{L}f}(\varepsilon \mp eV) - \mathbf{\Gamma}^{\mathcal{R}f}(\varepsilon)\big] \\ & \widehat{\mathbf{G}}^{<}_{c,c}(\varepsilon) + \big[\hat{\mathbf{\Gamma}}^{\mathcal{L}f}(\varepsilon \mp eV)\mathbf{f}_{\mathcal{L}}(\varepsilon \mp eV) - \\ & \mathbf{\Gamma}^{\mathcal{R}f}(\varepsilon)\mathbf{f}_{\mathcal{R}}(\varepsilon)\big]\big[\widehat{\mathbf{G}}^{r}_{c,c}(\varepsilon) - \widehat{\mathbf{G}}^{a}_{c,c}(\varepsilon)\big]\Big)_{ii}\Big\}, \qquad (33)\end{aligned}$$

where $\hat{\mathbf{\Gamma}}^{\mathcal{L}f} = \mathbf{R}^{f\dagger}(\frac{\theta_f}{2})\mathbf{\Gamma}^{\mathcal{L}f}\mathbf{R}^{f}(\frac{\theta_f}{2})$, $\theta_f = \theta_{\mathcal{L}f} - \theta_{\mathcal{R}f}$, and

$$\begin{aligned}\widehat{\mathbf{G}}^{r,a/<}_{c,c}(\varepsilon) \;=\; & \int d(t-t')e^{i\varepsilon(t-t')/\hbar}\mathbf{P}(\mu_{\mathcal{R}\mathcal{C}}t)\mathbf{R}^{f}(\frac{\theta_{\mathcal{R}f}}{2}) \\ & \mathbf{G}^{r,a/<}_{c,c}(t,t')\mathbf{R}^{f\dagger}(\frac{\theta_{\mathcal{R}f}}{2})\mathbf{P}^{\dagger}(\mu_{\mathcal{R}\mathcal{C}}t'), \\ \mathbf{f}_{\gamma}(\varepsilon \mp c) \;=\; & \\ & \begin{pmatrix} f(\varepsilon - c) & 0 & 0 & 0 \\ 0 & f(\varepsilon + c) & 0 & 0 \\ 0 & 0 & f(\varepsilon - c) & 0 \\ 0 & 0 & 0 & f(\varepsilon + c) \end{pmatrix}.\end{aligned}$$

The expression of tunneling current (33) resembles formally the current formula derived by Meir and Wingreen[12] for a confined region coupled to two normal electrodes. The difference lies in that the coupling matrices and Green functions in (33) are spanned in the Nambu-spinor space, which reflects the dependence of the current on the spin polarization of the ferromagnetic leads and the relative orientation of the magnetic moments. When we set to zero the magnetic moments of the two leads, Eq. (33) reduces to Equation (5) in the paper of Meir and Wingreen,[12] since in this case the ferromagnetic leads become normal metals. As seen from Eq. (33), current is only dependent on the relative orientation of the magnetizations of two leads, although there is an apparent $\theta_{\mathcal{R}f}$ dependence in the expression for $\widehat{\mathbf{G}}^{r,a/<}$. Nevertheless, this dependence of the Green functions $\widehat{\mathbf{G}}^{r,a/<}$ on the orientation of the ferromagnet magnetization comes from the self-energy matrices $\widehat{\Sigma}^{\mathcal{L}f}$ and $\widehat{\Sigma}^{\mathcal{R}f}$ after the *rotation* operation $\mathbf{R}^{f}(\frac{\theta_{\mathcal{R}f}}{2})$, hence they only depend on the relative orientation as can be seen more clearly in the non-interacting model.

If one lead ($\mathcal{L}$) is ferromagnetic and the other ($\mathcal{R}$) is superconducting it is expected that Andreev reflection process, dependent on the spin polarization of the ferromagnet, will dominate the current at low bias voltages. Applying a *phase* and a *rotation* transformations to Eq. (31), simple integration gives

$$\begin{aligned}\mathcal{I}_{fns} \;=\; & \frac{ie}{2\hbar}\sum^{i=1,3}\int\frac{d\varepsilon}{2\pi}\mathrm{Tr}\Big\{\Big(\big[\mathbf{\Gamma}^{\mathcal{L}f}(\varepsilon \mp eV) - \mathbf{\Gamma}^{\mathcal{R}s}_{\rho}(\varepsilon)\big] \\ & \breve{\mathbf{G}}^{<}_{c,c}(\varepsilon) + \big[\mathbf{\Gamma}^{\mathcal{L}f}(\varepsilon \mp eV)\mathbf{f}_{\mathcal{L}}(\varepsilon \mp eV) - \\ & \mathbf{\Gamma}^{\mathcal{R}s}_{\rho}(\varepsilon)\mathbf{f}_{\mathcal{R}}(\varepsilon)\big]\big[\breve{\mathbf{G}}^{r}_{c,c}(\varepsilon) - \breve{\mathbf{G}}^{a}_{c,c}(\varepsilon)\big]\Big)_{ii}\Big\}, \qquad (34)\end{aligned}$$

in which the full Green functions are

$$\begin{aligned}\breve{\mathbf{G}}^{r,a/<}_{c,c}(\varepsilon) \;=\; & \int d(t-t')e^{i\varepsilon(t-t')/\hbar}\mathbf{P}(\mu_{\mathcal{R}\mathcal{C}}t + \frac{\varphi_{\mathcal{R}}}{2}) \\ & \mathbf{R}^{f}(\frac{\theta_{\mathcal{L}f}}{2})\mathbf{G}^{r,a/<}_{c,c}(t,t')\mathbf{R}^{f\dagger}(\frac{\theta_{\mathcal{L}f}}{2})\mathbf{P}^{\dagger}(\mu_{\mathcal{R}\mathcal{C}}t' + \frac{\varphi_{\mathcal{R}}}{2}).\end{aligned}$$

In Eq. (34) the current does not depend on the orientation of the magnetization of the ferromagnetic lead and the phase of the order parameter of the superconductor lead. This can be clearly demonstrated by expanding the full Green functions of the central part perturbatively, as we will show below in the non-interacting case. In addition, one can divide the current into several parts implying the contributions from different physical processes such as normal particle tunneling and Andreev reflection, after expanding the right hand side of Eq. (34). We will show it later in the non-interaction case.

When two leads are superconducting, the situation becomes much more complicated. As did in the previous examples, we derive the following current formula for $S/I/N/I/S$ or $S-QD-S$ systems

$$\begin{aligned}\mathcal{I}_{sns}(t) \;=\; & -\frac{e}{\hbar}\sum^{i=1,3}\int\frac{d\varepsilon}{2\pi}\mathrm{ImTr}\Big\{\Big(\frac{1}{2}\big[\tilde{\mathbf{\Gamma}}^{\mathcal{L}s}_{\varrho}(\varepsilon \mp eV;t) - \\ & \mathbf{\Gamma}^{\mathcal{R}s}_{\varrho}(\varepsilon)\big]\widetilde{\mathbf{G}}^{<}_{c,c}(\varepsilon;t) - \big[\tilde{\mathbf{\Gamma}}^{\mathcal{L}s}_{\rho}(\varepsilon \mp eV;t) \\ & \mathbf{f}_{\mathcal{L}}(\varepsilon \mp eV) - \mathbf{\Gamma}^{\mathcal{R}s}_{\rho}(\varepsilon)\mathbf{f}_{\mathcal{R}}(\varepsilon)\big]\widetilde{\mathbf{G}}^{a}_{c,c}(\varepsilon;t)\Big)_{ii}\Big\}, \qquad (35)\end{aligned}$$

where

$$\begin{aligned}\tilde{\mathbf{\Gamma}}^{\mathcal{L}s}_{\varrho/\rho}(\varepsilon \mp eV;t) \;=\; & \mathbf{P}^{\dagger}(eVt + \frac{\varphi_s}{2})\mathbf{\Gamma}^{\mathcal{L}s}_{\varrho/\rho}(\varepsilon \mp eV) \\ & \mathbf{P}(eVt + \frac{\varphi_s}{2}), \\ \widetilde{\mathbf{G}}^{r,a/<}_{c,c}(\varepsilon;t) \;=\; & \int d(t-t')e^{i\varepsilon(t-t')/\hbar}\mathbf{P}(\mu_{\mathcal{R}\mathcal{C}}t + \frac{\varphi_{\mathcal{R}}}{2}) \\ & \mathbf{G}^{r,a/<}_{c,c}(t,t')\mathbf{P}^{\dagger}(\mu_{\mathcal{R}\mathcal{C}}t' + \frac{\varphi_{\mathcal{R}}}{2}),\end{aligned}$$

with $\varphi_s = \varphi_{\mathcal{L}} - \varphi_{\mathcal{R}}$. One may wonder why we use the notation $\widetilde{\mathbf{G}}^{r,a/<}_{c,c}(\varepsilon;t)$ with the additional variable t other than $\widehat{\mathbf{G}}^{r,a/<}_{c,c}(\varepsilon)$. The reason is that the full Green functions $\mathbf{G}_{c,c}^{r,a/<}$ should be calculated in the presence of tunneling between the central part and the two sides, as well as the interactions in the central region. In the present case, the t-dependence can not be avoided in the self-energy matrices, while it can be removed by a unitary *phase* operation when only one superconductor is involved. The current through a confined interacting region connected to two superconductor leads is generally time dependent, as in the case of biased weak Josephson links.[31] However, in the limiting case of zero bias, the current is a time-independent nonzero quantity, as can be seen from Eq. (35). In other theoretical treatments,[13,42] a double-time Fourier transformation is usually taken as $X(t,t') = \frac{1}{2\pi}\sum_n \int d\omega e^{-i\omega t} e^{i(\omega+n\omega_0/2)t'} X(\omega, \omega+n\omega_0/2)$, where $\omega_0 = 2eV/\hbar$, and the current yields a harmonic expansion of the fundamental frequency $\mathcal{I}(t) = \sum_n I_n e^{in\omega_0 t}$. In fact, the Green functions $\widetilde{\mathbf{G}}_{d,d}^{r,a/<}$ in (35) can be expanded in powers of the fundamental frequency ω_0, i.e., $\widetilde{\mathbf{G}}_{d,d}^{r,a/<}(\varepsilon,t) = \sum_m \widetilde{\mathbf{G}}_{d,d}^{r,a/<}(\varepsilon,\varepsilon+m\omega_0/2)e^{im\omega_0 t/2}$, which with the expression for the Green function $\widetilde{\mathbf{G}}_{d,d}^{r,a/<}$ below Eq.(35) is exactly of the form of the double-energy transformation.[42] However, we show here that one can obtain *in principle* the time dependence of the current, as long as one can derive the full Green functions of the central part, which need further investigation.

So far we have presented a general formulation to calculate the current through a confined normal region connected to two leads being either ferromagnetic or superconducting, and the Meir-Wingreen-type formulae in the specific cases. Although the formalism can not applied to the strong coupling of the central normal part to the outer world as the circuit theory of the hybrid mesoscopic transport,[20] it permits us to investigate the effects of the single particle interference and strong electron-electron interaction on the transport properties of hybrid mesoscopic systems, which is ignored in the circuit theory. Compared to the other formalisms based on the similar Keldysh NEGF technique,[9,12,15,16,17,67] our formalism is more systematic and more general. In the present formalism, one do not need to make additional ad hoc assumptions as mentioned in the introduction. One can also judge what quantities can be measured in experiment in a much more complicated structure, by observing simply the energy-independent arguments in the exponential functions or the triangle functions in the unitary matrices of the tunneling parts of the Hamiltonian after the Bogoliubov transformations. As we will demonstrate, we obtain the final current formula after simple matrix algebra rather than difficult mathematical techniques.[15,16,17,67] This kind of mathematical simplicity makes our formalism more appearing than others. More importantly, an explicit energy- and bias-voltage dependence of the level-width functions and distribution functions allows us to investigate the I-V characteristics in a much more wider range of bias voltage.

III. APPLICATIONS TO THE NONINTERACTING MODEL IN THE CENTRAL REGION

In this section we use the formulae developed above to study transport properties of various kinds of hybrid mesoscopic systems in which, for simplicity and convenience of comparison with other theories, the interaction effects in the central confined region are not considered. The absence of the interactions permits an analysis of the genuine physical influence of ferromagnetism and superconductor proximity on the transport properties in hybrid structures. One of the best candidates for a non-interaction confined region is double-barrier resonant structures (DBTSs) with quantized discrete energy levels.[4] Therefore we adopt the double-barrier model with the emitter and collector replaced by either a ferromagnet or a superconductor. Throughout the following calculations we use the following approximations: (i) the level shift is omitted, (ii) the coupling coefficients are real constants, independent of spin and energy such that $V_{kn;\sigma}^{\gamma f/s} = V^{\gamma f/s} = V^{\gamma f/s*}$. However, we will abandon the usual[9,12,14,15,16] wide-band approximation of the level-width functions which is reasonable in the low-voltage transport, since in this paper we also deal with high bias voltage situation. As we will show, this permits us to investigate the current within a much wider region of bias voltage and find interesting transport features of the same resonant structures which can not be found in the other formalisms based on the Keldysh NEGF technique.[15,16,17]

In the absence of interactions within the intermediate normal metal, the full retarded/advanced Green function can be solved from Dyson equation

$$\begin{aligned}
\mathbf{G}_{c,c}^{r/a}(t,t') &= \mathbf{G}_{c,c}^{0r/a}(t,t') + \int dt_1 \int dt_2 \mathbf{G}_{c,c}^{0r/a}(t,t_1) \\
&\qquad \mathbf{\Sigma}^{r/a}(t_1,t_2)\mathbf{G}_{c,c}^{r/a}(t_2,t') \\
&= \mathbf{G}_{c,c}^{0r/a}(t,t') + \int dt_1 \int dt_2 \mathbf{G}_{c,c}^{r/a}(t,t_1) \\
&\qquad \mathbf{\Sigma}^{r/a}(t_1,t_2)\mathbf{G}_{c,c}^{0r/a}(t_2,t'), \qquad (36)
\end{aligned}$$

in which $\mathbf{G}_{c,c}^{0r/a}$ is the decoupled Green function, which becomes when the central region is isolated from the outside world

$$\mathbf{g}^{r/a}_{c,c}(t,t') = \mp i\vartheta(\pm t_1 \mp t_2)\sum_n \begin{pmatrix} e^{-i(\varepsilon_{n\uparrow}-\mu_C)(t_1-t_2)/\hbar} & 0 & 0 & 0 \\ 0 & e^{i(\varepsilon_{n\downarrow}-\mu_C)(t_1-t_2)/\hbar} & 0 & 0 \\ 0 & 0 & e^{-i(\varepsilon_{n\downarrow}-\mu_C)(t_1-t_2)/\hbar} & 0 \\ 0 & 0 & 0 & e^{i(\varepsilon_{n\uparrow}-\mu_C)(t_1-t_2/\hbar)} \end{pmatrix}. \tag{37}$$

The lesser/greater Green function of the central region is calculated via Keldysh equation

$$\begin{aligned} \mathbf{G}^{</>}_{c,c}(t,t') \;=\; & \int dt_1 \int dt_2 \int dt_3 \int dt_4 \\ & \left[\mathbf{1} + \mathbf{G}^r_{c,c}(t,t_1)\mathbf{\Sigma}^r(t_1,t_2)\right] \\ & \mathbf{G}^{0</>}_{c,c}(t_2,t_3) \\ & \left[\mathbf{1} + \mathbf{\Sigma}^a(t_3,t_4)\mathbf{G}^a_{c,c}(t_4,t')\right] + \\ & \int dt_1 \int dt_2 \mathbf{G}^r_{c,c}(t,t_1) \\ & \qquad \mathbf{\Sigma}^{</>}(t_1,t_2)\mathbf{G}^a_{c,c}(t_2,t'). \end{aligned} \tag{38}$$

Once the full Green functions in the central region are known, we then have the complete knowledge to investigate tunneling processes in the specific structures. In the following we study electron tunneling in three typical hybrid structures: (a) $F/I/N/I/F$ magnetic DBTSs, (b) $F/I/N/I/S$ DBTSs, and (c) $S/I/N/I/S$ DBTSs.

A. F/I/N/I/F structures

When two ferromagnets are separated by a thin nonmagnetic barrier, two kinds of physical effects arise. The first is the *spin valve* effect,[35,38] showing a $(1+\varepsilon\cos\theta)$ dependence of the tunnel conductance on the relative orientation θ between the involved two magnetizations. The other is tunnel magnetoresistance (TMR),[35] defined by $\Delta R/R = (R_a - R_p)/R_a$, where R_p and R_a are the resistances when two magnetizations are parallel and antiparallel, respectively. The *spin valve* and TMR are due to the spin polarization induced by an exchanging coupling between electron spins and the internal magnetization,[35,38] and the relative orientation of the magnetizations can be adjusted by applying a magnetic field. A TMR up to 11.8% at room temperatures, and 24% at $4.2K$, was reported in $CoFe/Al_2O_3/Co$ planar magnetic junctions.[43] It is observed that the TMR decreases with increasing bias voltage.[43]

Recently, double-barrier magnetic resonant structures has attracted much experimental[44] and theoretical[16,45,46,47,48,49] attention. The theoretical results show that the TMR of resonant magnetic structures is enhanced compared to the single magnetic junctions due to resonant tunneling.[45,46,47,48,49] However, there appears a controversial issue related to the TMR enhancement, on whether it is for peak[45] or valley current.[46] In addition, Sheng et al.[47] found both positive and negative TMR in $F/I/F/I/F$ double junctions. To clarify these issues, we re-examine this problem using our formula (33) in terms of the two-band free-electron spin-polarization model[38] for the ferromagnetic leads. A typical double-barrier magnetic structure is schematically plotted in Fig. 2.

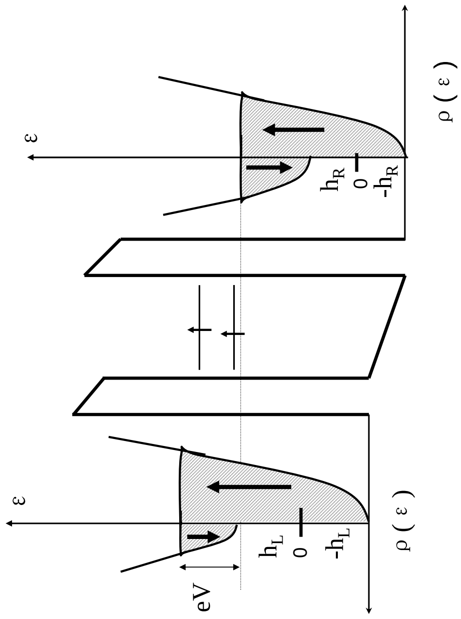

FIG. 2: A schematic potential profile for a biased magnetic double-barrier structure with two ferromagnetic electrodes characterized by their respective magnetizations $h_{\mathcal{L}}$ and $h_{\mathcal{R}}$. The hatched regions denote the states occupied by electrons.

We take two steps to calculate the full retarded/advanced Green function $\mathbf{G}^{r/a}_{c,c}(t,t')$ of the central region. First we decouple the system from the left ferromagnet, denoting the corresponding retarded/advanced Green function by $\mathcal{G}^{r/a}_{c,c}(t,t')$, then we couple the central region to the left ferromagnet and calculate the full

Green function $\mathbf{G}$ from $\mathcal{G}$. From the Dyson equation (36) we have

$$\begin{aligned}\widehat{\mathbf{G}}^{r/a}_{c,c}(t,t') &= \widehat{\mathcal{G}}^{r/a}_{c,c}(t,t') + \int dt_1 \int dt_2 \widehat{\mathcal{G}}^{r/a}_{c,c}(t,t_1) \\ &\qquad \widehat{\mathbf{\Sigma}}^{r/a}_{\mathcal{L}f}(t_1,t_2)\widehat{\mathbf{G}}^{r/a}_{c,c}(t_2,t'), \qquad (39)\\ \widehat{\mathcal{G}}^{r/a}_{c,c}(t,t') &= \widehat{\mathbf{g}}^{r/a}_{c,c}(t,t') + \int dt_1 \int dt_2 \widehat{\mathbf{g}}^{r/a}_{c,c}(t,t_1) \\ &\qquad \widehat{\mathbf{\Sigma}}^{r/a}_{\mathcal{R}f}(t_1,t_2)\widehat{\mathcal{G}}^{r/a}_{c,c}(t_2,t'), \qquad (40)\end{aligned}$$

where ($\mathbf{X} = \mathbf{G}^{r,a/<}, \mathcal{G}^{r,a/<}, \mathbf{g}^{r,a/<}$ and $\mathbf{\Sigma}^{r,a/<}$)

$$\widehat{\mathbf{X}}(t,t') = \mathbf{P}(\mu_{\mathcal{RC}}t)\mathbf{R}^f(\frac{\theta_{\mathcal{R}f}}{2})\mathbf{X}(t,t')\mathbf{R}^{f\dagger}(\frac{\theta_{\mathcal{R}f}}{2})\mathbf{P}^\dagger(\mu_{\mathcal{RC}}t').$$

Substituting the self-energy matrices $\mathbf{\Sigma}^{r/a}_{\mathcal{R}f}$ (Appendix A) into the Dyson equation (40), one has

$$\begin{aligned}\widehat{\mathcal{G}}^{r/a}_{c,c}(t,t') &= \int \frac{d\varepsilon}{2\pi} e^{-i\varepsilon(t-t')/\hbar}\Big[\widehat{\mathbf{g}}^{r/a-1}_{c,c}(\varepsilon) \pm \frac{i}{2}\mathbf{\Gamma}^{\mathcal{R}f}(\varepsilon)\Big]^{-1} \\ &= \int \frac{d\varepsilon}{2\pi} e^{-i\varepsilon(t-t')/\hbar}\widehat{\mathcal{G}}^{r/a}_{c,c}(\varepsilon), \qquad (41)\end{aligned}$$

where the retarded/advanced Green function for the isolated central region is

$$\widehat{\mathbf{g}}^{r/a}_{c,c}(\varepsilon) = \begin{pmatrix} (\sum\limits_n \frac{1}{\varepsilon-\epsilon'_{n\uparrow}\pm i0^+})^{-1} & 0 & 0 & 0 \\ 0 & (\sum\limits_n \frac{1}{\varepsilon+\epsilon'_{n\downarrow}\pm i0^+})^{-1} & 0 & 0 \\ 0 & 0 & (\sum\limits_n \frac{1}{\varepsilon-\epsilon'_{n\downarrow}\pm i0^+})^{-1} & 0 \\ 0 & 0 & 0 & (\sum\limits_n \frac{1}{\varepsilon+\epsilon'_{n\uparrow}\pm i0^+})^{-1} \end{pmatrix}, \qquad (42)$$

with $\epsilon'_{n\sigma} = \varepsilon_{n\sigma} - \mu_{\mathcal{C}} + \mu_{\mathcal{R}}$. The full retarded/advanced Green function is obtained in the same way

$$\begin{aligned}\widehat{\mathbf{G}}^{r/a}_{c,c}(t,t') &= \int \frac{d\varepsilon}{2\pi} e^{-i\varepsilon(t-t')/\hbar}\Big[\widehat{\mathcal{G}}^{r/a-1}_{c,c}(\varepsilon) \pm \\ &\qquad \frac{i}{2}\hat{\mathbf{\Gamma}}^{\mathcal{L}f}(\varepsilon \mp eV)\Big]^{-1} \\ &= \int \frac{d\varepsilon}{2\pi} e^{-i\varepsilon(t-t')/\hbar}\Big[\widehat{\mathbf{g}}^{r/a-1}_{c,c}(\varepsilon) \pm \frac{i}{2} \\ &\qquad \mathbf{\Gamma}^{\mathcal{R}f}(\varepsilon) \pm \frac{i}{2}\hat{\mathbf{\Gamma}}^{\mathcal{L}f}(\varepsilon \mp eV))\Big]^{-1} \\ &= \int \frac{d\varepsilon}{2\pi} e^{-i\varepsilon(t-t')/\hbar}\widehat{\mathbf{G}}^{r/a}_{c,c}(\varepsilon). \qquad (43)\end{aligned}$$

The lesser Green function is associated with the retarded and advanced Green functions via the Keldysh equation (38) where $\hat{\mathbf{g}}^<(t,t') = 0$

$$\begin{aligned}\widehat{\mathbf{G}}^{<}_{c,c}(t,t') &= \int dt_1 \int dt_2 \widehat{\mathbf{G}}^r_{c,c}(t,t_1)\Big[\widehat{\mathbf{\Sigma}}^{</>}_{\mathcal{L}f}(t_1,t_2) \\ &\qquad + \widehat{\mathbf{\Sigma}}^{</>}_{\mathcal{R}f}(t_1,t_2)\Big]\widehat{\mathbf{G}}^a_{c,c}(t_2,t') \\ &= \int \frac{d\varepsilon}{2\pi} e^{-i\varepsilon(t-t')/\hbar}\widehat{\mathbf{G}}^r_{c,c}(\varepsilon)\big[\hat{\mathbf{\Gamma}}^{\mathcal{L}f}(\varepsilon \mp eV) \\ &\qquad \mathbf{f}_{\mathcal{L}}(\varepsilon \mp eV) - \mathbf{\Gamma}^{\mathcal{R}f}(\varepsilon)\mathbf{f}_{\mathcal{R}}(\varepsilon)\big]\widehat{\mathbf{G}}^a_{c,c}(\varepsilon) \\ &= \int \frac{d\varepsilon}{2\pi} e^{-i\varepsilon(t-t')/\hbar}\widehat{\mathbf{G}}^<_{c,c}(\varepsilon). \qquad (44)\end{aligned}$$

Substituting the advanced and lesser Green functions (43) and (44) into Eq. (33) or (31), one gets the following Landauer-Büttiker-type[5] formula for the current through a non-interacting $F/I/N/I/F$ magnetic structure,

$$\mathcal{I}_{fnf}(\theta_f) = \frac{2e}{h}\int d\varepsilon[f_{\mathcal{L}}(\varepsilon - eV) - f_{\mathcal{R}}(\varepsilon)]\mathcal{T}_{fnf}(\varepsilon,\theta_f), \qquad (45)$$

where the transmission coefficient $\mathcal{T}_{fnf}$ is cast into the following compact form

$$\begin{aligned}&\mathcal{T}_{fnf}(\varepsilon,\theta_f) \\ &= \frac{1}{2}\sum_{i=1,3}\Big(\hat{\mathbf{\Gamma}}^{\mathcal{L}f}(\varepsilon \mp eV)\widehat{\mathbf{G}}^r_{c,c}(\varepsilon)\mathbf{\Gamma}^{\mathcal{R}f}(\varepsilon)\widehat{\mathbf{G}}^a_{c,c}(\varepsilon)\Big)_{ii} \\ &= \frac{1}{2}\Big[(\cos^2\frac{\theta_f}{2}\hat{\Gamma}^{\mathcal{L}f}_\uparrow\Gamma^{\mathcal{R}f}_\uparrow + \sin^2\frac{\theta_f}{2}\hat{\Gamma}^{\mathcal{L}f}_\downarrow\Gamma^{\mathcal{R}f}_\uparrow)|\widehat{G}^r_{c,c;11}|^2 \\ &\quad -(2\Gamma^{\mathcal{R}f}_\uparrow\Gamma^{\mathcal{R}f}_\downarrow + \cos^2\frac{\theta_f}{2}\hat{\Gamma}^{\mathcal{L}f}_\downarrow\Gamma^{\mathcal{R}f}_\uparrow + \sin^2\frac{\theta_f}{2}\hat{\Gamma}^{\mathcal{L}f}_\uparrow\Gamma^{\mathcal{R}f}_\uparrow) \\ &\quad |\widehat{G}^r_{c,c;13}|^2 - (2\Gamma^{\mathcal{R}f}_\uparrow\Gamma^{\mathcal{R}f}_\downarrow + \cos^2\frac{\theta_f}{2}\hat{\Gamma}^{\mathcal{L}f}_\uparrow\Gamma^{\mathcal{R}f}_\downarrow + \\ &\quad \sin^2\frac{\theta_f}{2}\hat{\Gamma}^{\mathcal{L}f}_\downarrow\Gamma^{\mathcal{R}f}_\downarrow)|\widehat{G}^r_{c,c;31}|^2 + (\cos^2\frac{\theta_f}{2}\hat{\Gamma}^{\mathcal{L}f}_\downarrow\Gamma^{\mathcal{R}f}_\downarrow + \\ &\quad \sin^2\frac{\theta_f}{2}\hat{\Gamma}^{\mathcal{L}f}_\uparrow\Gamma^{\mathcal{R}f}_\downarrow)|\widehat{G}^r_{c,c;33}|^2\Big]. \qquad (46)\end{aligned}$$

Notice that we have dropped the arguments $\varepsilon - eV$ in $\hat{\Gamma}^{\mathcal{L}f}_\sigma$ and ε in $\Gamma^{\mathcal{R}f}_\sigma$ for brevity. The full retarded Green function in Eq. (46) is determined by the matrix inversion $\widehat{\mathbf{G}}^r_{c,c} = [\widehat{\mathbf{g}}^{r-1}_{c,c} + \frac{i}{2}\hat{\mathbf{\Gamma}}^{\mathcal{L}f} + \frac{i}{2}\mathbf{\Gamma}^{\mathcal{R}f}]^{-1}$, and we have

$$\widehat{G}^r_{c,c;11} = \widehat{G}^{-1}_{ff}(\varepsilon)\Big[(\sum_n \frac{1}{\varepsilon - \epsilon'_{n\downarrow} + i0^+})^{-1} +$$

$$
\begin{aligned}
&\qquad \frac{i}{2}(\cos^2\frac{\theta_f}{2}\hat{\Gamma}_{\downarrow}^{\mathcal{L}f}+\sin^2\frac{\theta_f}{2}\hat{\Gamma}_{\uparrow}^{\mathcal{L}f}+\Gamma_{\downarrow}^{\mathcal{R}f})\Big],\\
\widehat{G}^r_{c,c;13} &= \widehat{G}^r_{c,c;31}=\frac{-\frac{i}{4}\sin\theta_f(\hat{\Gamma}_{\uparrow}^{\mathcal{L}f}-\hat{\Gamma}_{\downarrow}^{\mathcal{L}f})}{\widehat{G}_{ff}(\varepsilon)},\\
\widehat{G}^r_{c,c;33} &= \widehat{G}^{-1}_{ff}(\varepsilon)\Big[(\sum_n\frac{1}{\varepsilon-\epsilon'_{n\uparrow}+i0^+})^{-1}+\\
&\qquad \frac{i}{2}(\cos^2\frac{\theta_f}{2}\hat{\Gamma}_{\uparrow}^{\mathcal{L}f}+\sin^2\frac{\theta_f}{2}\hat{\Gamma}_{\downarrow}^{\mathcal{L}f}+\Gamma_{\uparrow}^{\mathcal{R}f})\Big],\\
\widehat{G}_{ff}(\varepsilon) &= \widehat{G}^r_{c,c;11}\widehat{G}^r_{c,c;33}-\widehat{G}^r_{c,c;13}\widehat{G}^r_{c,c;31}.
\end{aligned}
$$

To obtain the last equality of Eq. (46), we have used

$$
\begin{aligned}
(\widehat{g}^{r/a-1}_{c,c;11}\pm\frac{i}{2}\Gamma^f_{11})\widehat{G}^{r/a}_{c,c;13} &= \pm\frac{i}{2}\Gamma^f_{13}\widehat{G}^{r/a}_{c,c;33}\\
(\widehat{g}^{r/a-1}_{c,c;33}\pm\frac{i}{2}\Gamma^f_{33})\widehat{G}^{r/a}_{c,c;31} &= \pm\frac{i}{2}\Gamma^f_{31}\widehat{G}^{r/a}_{c,c;11},
\end{aligned}
$$

where $\mathbf{\Gamma}^f=\hat{\mathbf{\Gamma}}^{\mathcal{L}f}+\mathbf{\Gamma}^{\mathcal{R}f}$.

One sees from Eqs. (45) and (46) that the current has a generic dependence on the relative orientation θ_f between the two magnetizations. By observing the current expression and scrutinizing the structure of the Green functions, it is not difficult to find that the tunneling current through the magnetic structure is generally maximized at $\theta_f=0$ (parallel magnetization) and minimized at $\theta_f=\pi$ (antiparallel magnetization), a typical *spin valve* effect also in magnetic resonant tunneling devices (data not shown here). The ferromagnetism is reflected in the θ_f- and $\Gamma^{\gamma f}_{\sigma}$-dependence of the full Green functions of the central part $\hat{G}_{c,c}$, as well the transmission function $\mathcal{T}$. When at least one lead is nonmagnetic, the θ_f-dependence can be removed with the help of a *rotation* operation $\mathbf{R}^f$. If we set $\Gamma^{\mathcal{L}f}_{\uparrow}=\Gamma^{\mathcal{L}f}_{\downarrow}$ and $\Gamma^{\mathcal{R}f}_{\uparrow}=\Gamma^{\mathcal{R}f}_{\downarrow}$, the current formula (45) will recover the usual Landauer-Büttiker formula and the transmission is finally simplified to the Breit-Wigner type in the single level case. We notice that the current formula (45) is formally similar to the results of Wang et al.[16] and Zhu et al.,[17] however, the discrepancy is nontrivial. The current formula (45) allows us to calculate the I-V curves in a much wider region of bias voltage yielding rich physics, while according to the theoretical treatments of Wang et al.[16] and Zhu et al.,[17] the current formula is restricted to the low bias voltage case where the level-width functions can be viewed as energy-independent constants, and thus may result in even wrong consequences in the large bias voltage limit.

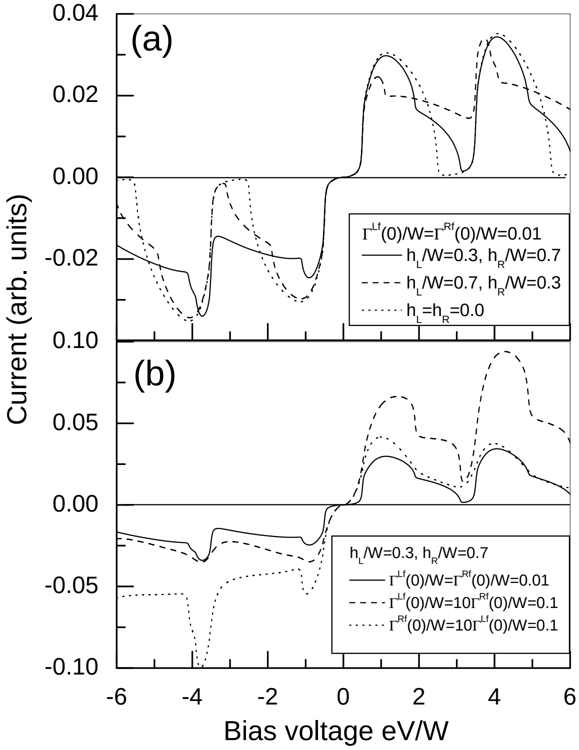

FIG. 3: I-V characteristics of a magnetic double-barrier structure for (a) different magnetizations $h_{\mathcal{L}}$ and $h_{\mathcal{R}}$ and (b) different couplings $\Gamma^{\mathcal{L}f}(0)$ and $\Gamma^{\mathcal{R}f}(0)$ at temperature $k_BT=0.1W$. The level spacing is $1.5W$, larger than the bandwidth W.

Of particular interest is the current-voltage characteristics of double-barrier structures. In subsequent calculations, we approximate the density of states of the ferromagnetic leads by that of the two-band free-electron spin-polarization model[38,46] and take into consideration the finite width of these two bands. In this model the dimensionless DOS of the spin bands is $\rho^{\gamma f}_{\sigma}(\varepsilon)\propto\sqrt{(\varepsilon+\sigma h_\gamma+W)/W}$, where W is the bandwidth measured from the band bottom to the Fermi level. For some ferromagnetic metals, this is quite an appropriate approximation.[38,50,51] In the absence of a magnetic field in the central region, $\varepsilon_{n\uparrow}=\varepsilon_{n\downarrow}=\varepsilon_n$. To model the bias voltage drop inside the well we take $\mu_{\mathcal{C}}=\mu_{\mathcal{R}}-eV/2$, since the bias potential is assumed distributing uniformly across the double-barrier structure. Without any loss of generality we consider two quasi-stationary levels in the well, of which the energy of the lowest one is $0.25W$ when $V=0$ and the level spacing is chosen as $1.5W$, larger than the bandwidth of the ferromagnets. This assumption is, in practice, quite reasonable for the narrow-band ferromagnetic metals and quantum wells with very large level spacing or small quantum dots with very large charging energy. The I-V curves are shown in Fig. 3. The dotted line in Fig. 3(a), the well-known I-V characteristics of usual double-barrier structures, is given for comparison with the ferromagnetic case. In the presence of ferromagnets, the structure of resonant shoulders neighboring to resonant peaks is celebrated in the I-V plots. The ratio of the peak width to the shoulder width is about $(W-h_\gamma)/2h_\gamma$. Moreover, the valley current in a normal resonant tunneling structure is lifted when the leads become ferromagnetic. These surprising results, unexpected within the wide-band approximation, can be understood from the potential profile of this kind of magnetic double junction structure, shown in Fig. 2. It is well known that the current through a usual double-barrier structure is resonantly enhanced when one of the well levels falls into the region of a Fermi sea, i.e., $eV < \varepsilon_n + eV/2 < W + eV$.[52] In the ferromagnetic situation, the Fermi sea is distorted and comprises two distinct parts: one with both spin-up and spin-down bands, and the other with only a spin-up or spin-down band, as displayed in Fig. 2. We thus have two types of Fermi sea for ferromagnets, one is represented by $h_\gamma + eV < \varepsilon_n + eV/2 < W + eV$ and the other is $-h_\gamma + eV < \varepsilon_n + eV/2 < h_\gamma + eV$. It is obvious that the resonant current through one of the well levels being within the sea of the first type is larger than that of the second type, which is clearly reflected in the I-V characteristics in Fig. $3(a)$.

Next we investigate the influence of coupling asymmetry on the tunneling current. The results are presented in Fig. $3(b)$. The magnitude of resonant current is significantly enhanced when one of the couplings becomes 10 times as large. The coupling asymmetry induces a more significant enhancement of the tunneling current if it is the coupling to the higher-voltage lead (emitter) that is stronger, consistent with the tight-binding numerical result in the usual DBTS.[53] The ferromagnetic I-V characteristics (peaks plus shoulders) in the reverse-bias case is blurred, also due to the same coupling asymmetry effect. These features can be understood in a similar way. The resonant current is roughly proportional to the ratio $\Gamma^{\mathcal{L}f}(0)\rho^{\mathcal{L}f}\Gamma^{\mathcal{R}f}(0)\rho^{\mathcal{R}f}/(\Gamma^{\mathcal{L}f}(0)\rho^{\mathcal{L}f} + \Gamma^{\mathcal{R}f}(0)\rho^{\mathcal{R}f})^2$, which becomes larger when one of the couplings $\Gamma^{\mathcal{L}f}(0)$ or $\Gamma^{\mathcal{R}f}(0)$ is enhanced. However, the magnitude of this enhancement also depends on the DOS of the ferromagnet lead $\rho^{\gamma f}$. If one strengthens the coupling to the lower-voltage lead (collector), the tunneling current is slightly enhanced since the DOS of the collector is comparatively large.

Following Sheng et al.,[47] we define the tunnel magnetoresistance (TMR) as $\Delta R/R = [\mathcal{I}_{fnf}(\pi) - \mathcal{I}_{fnf}(0)]/\max(\mathcal{I}_{fnf}(\pi), \mathcal{I}_{fnf}(0))$. In Fig. 4 we give the TMR as a function of the bias voltage for some typical couplings, and the $I - V$ curves in the cases of parallel and antiparallel alignments of magnetizations for the convenience of comparison and analysis. In contrary to the monotonous decay with the bias voltage,[43] the TMR in magnetic DBTSs displays complex dependence on the bias voltage no matter what the values of couplings are, which arises from the resonant tunneling of electrons. This feature reveals that there is richer physics in the TMR of magnetic resonant structures. We notice also that the bias voltage dependence of the TMR can be comparatively simple if the collector ferromagnet is of low degree of spin polarization h_γ/W, as shown in the negative bias domains of Fig. 4. This phenomenon can be ascribed to the weak perturbation of the spin-up and spin-down DOS of the ferromagnet with small h_γ/W by an external magnetic field. In addition, the peculiar behavior of the TMR also depends on the strengths and symmetry of the elastic couplings. In the strong coupling case (Fig. $4(d)$), the TMR shows a resonant behavior similar to that in the tunneling current,[45,47] and can even be negative at some bias voltages.[47] In other cases (Fig. $4(a)$-(c)), the TMR drops within the resonant peak region and then develops peaks at the boundaries between the current peaks and shoulders, similar to the result of a non-interacting quantum dot coupled to two magnetic leads.[46] The different oscillatory behaviors of the TMR with the bias voltage for different couplings imply that the analysis on the TMR in the resonant structure[46] may not stand. It is worth noticing that the TMR will eventually decay to zero in the large bias voltage limit, due to the trivial dependence on the interchange of the spin-up and spin-down DOS of the lead at lower voltage. It is interesting to notice that the TMR reaches a maximum of 18% for asymmetric couplings. The maximum would increase further as the couplings become more asymmetric. The TMR ratio given by our simple model is consistent with the estimation for a resonant structure with Fe electrodes[51] and that of the Coulomb-blockade-free double junction model.[54] In magnetic resonant structures, TMR depends not only on the DOS of two electrodes as in the single junction case, but also on the spectral density of the central well associated with $\widehat{G}^r_{c,c}$, and thus exhibits complicated dependence on the bias voltage. As for the coupling dependence of peaks and valleys in the TMR curve, it is associated with the sensitivity to the distortion in the spin-up and spin-down DOS of the leads. Such a sensitivity strongly depends on the coupling strengths and which type of the Fermi sea the well levels fall into. In general, electrons in a one-band Fermi sea in the weak coupling case can detect much better the change in the DOS of the other ferromagnetic lead, and so the TMR develops a peak at the boundary between the two distinct types of Fermi sea.

To summarize this subsection, we have studied the I-V characteristics and TMR behavior in a double-barrier magnetic structure. It is found that both a peak and a shoulder emerge within the resonant region, manifesting directly the DOS profile of the ferromagnets. This finding may provide a new way to measure the degree of spin polarization of a ferromagnet. The TMR of resonant structures exhibits complex dependence on the bias voltage. It is either enhanced or suppressed, depending on the strengths and symmetry of the elastic couplings of the central region to the magnetic leads.

B. F/I/N/I/S structures

At an N/S interface a dissipative current in the normal metal can be converted into a dissipationless supercurrent in the superconductor via the Andreev reflection process.[29,30] Owing to the spin imbalance in the ferromagnet, the Andreev current is suppressed in a F/S contact.[36] Blonder, Tinkham and Klapwijk presented a one-dimensional model based on the Bogoliubov-de-

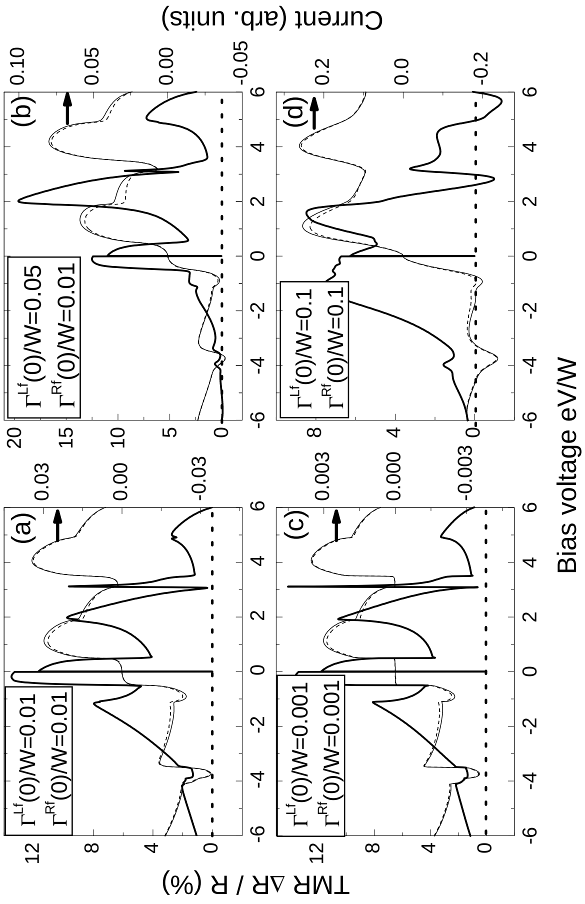

FIG. 4: TMR versus bias voltage of a magnetic double-barrier structure for different couplings at temperature $k_BT = 0.1W$. The thick lines are the results for TMR, and the thin solid and dashed lines represent the tunneling current with parallel and antiparallel magnetizations, respectively. The other parameters are the same as in Fig. 3.

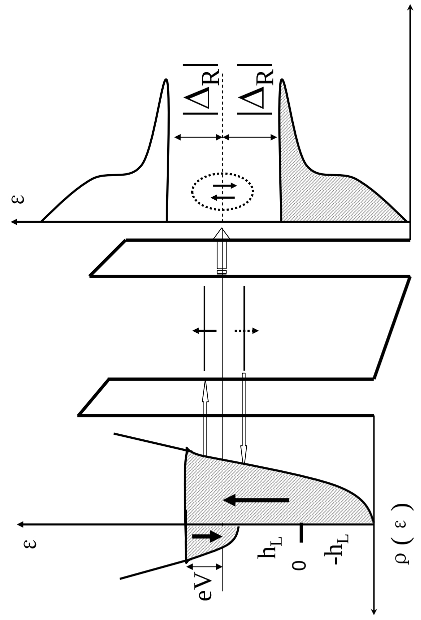

FIG. 5: A schematic potential profile for a biased DBTS connected to a ferromagnetic and a superconducting leads. The magnetization of the ferromagnetic lead is $h_{\mathcal{L}}$ and the energy gap of the superconductor is $|\Delta_{\mathcal{R}}|$. The hatched regions represent occupied electron states. A typical Andreev reflection process is shown: a spin-up electron above the chemical potential of the superconductor is reflected as a spin-down hole below the chemical potential at the NS interface, and finally into the ferromagnetic lead.

Gennes equation to analyze the transport processes at an N/S interface in terms of normal electron transmission and Andreev reflection probability, known as the BTK theory.[55] Cuevas et al. in 1996 also uncovered some kinds of electron tunneling processes in the N/S quantum point contacts within the Keldysh NEGF formalism starting from a microscopic Hamiltonian.[13] The scattering matrix theory[56,57] and Keldysh NEGF formalism[14,15] of electronic transport in $N-QD-S$ systems were also presented. Quite recently Zhu et al[17] investigated a $2F-QD-S$ structure using the Keldysh NEGF method, obtaining some interesting results. However, in the Keldysh NEGF treatment to the $N-QD-S$[14,15] or $2F-QD-S$,[17] they always made some assumptions that the ferromagnetic magnetization is along the z axis and the superconductor order parameter is a real quantity, and take the wide-band limit. Here we use the current formula (34) for $F/I/N/I/S$ systems to investigate the resonant Andreev current and I-V characteristics of a genuine non-interacting hybrid structure (see Fig. 5) beyond the wide-band limit.

Following similar procedures as in the last subsection, we derive the various kinds of full Green functions of the normal region for a noninteracting $F/I/N/I/S$ resonant structure as

$$\breve{\mathbf{G}}^{r,a/<}_{c,c}(t,t') = \int \frac{d\varepsilon}{2\pi} e^{-i\varepsilon(t-t')/\hbar} \breve{\mathbf{G}}^{r,a/<}_{c,c}(\varepsilon), \quad (47)$$

where ($\mathbf{X} = \mathbf{G}^{r,a/<}, \mathbf{g}^{r,a/<}$ and $\mathbf{\Sigma}^{r,a/<}$)

$$\breve{\mathbf{X}}(t,t') = \mathbf{P}(\mu_{\mathcal{RC}}t + \frac{\varphi_{\mathcal{R}}}{2})\mathbf{R}^f(\frac{\theta_{\mathcal{R}f}}{2})\mathbf{X}(t,t') \\ \mathbf{R}^{f\dagger}(\frac{\theta_{\mathcal{R}f}}{2})\mathbf{P}^\dagger(\mu_{\mathcal{RC}}t' + \frac{\varphi_{\mathcal{R}}}{2})$$

and

$$\breve{\mathbf{G}}^{r/a}_{c,c}(\varepsilon) = \Big[\breve{\mathbf{g}}^{r/a-1}_{c,c}(\varepsilon) \pm \frac{i}{2}\mathbf{\Gamma}^{\mathcal{R}s}_{\varrho}(\varepsilon) \pm$$

$$\frac{i}{2}\mathbf{\Gamma}^{\mathcal{L}f}(\varepsilon \mp eV)\Big]^{-1}, \quad (48)$$

$$\breve{\mathbf{G}}^{<}_{c,c}(\varepsilon) = \breve{\mathbf{G}}^{r}_{c,c}(\varepsilon)\big[\mathbf{\Gamma}^{\mathcal{L}f}(\varepsilon \mp eV)\mathbf{f}_{\mathcal{L}}(\varepsilon \mp eV) - \mathbf{\Gamma}^{\mathcal{R}s}_{\rho}(\varepsilon)\mathbf{f}_{\mathcal{R}}(\varepsilon)\big]\breve{\mathbf{G}}^{a}_{c,c}(\varepsilon).$$

Substituting the above Green functions into Eq. (34), we obtain

$$\begin{aligned}\mathcal{I}_{fns} &= \mathcal{I}^{A}_{fns} + \mathcal{I}^{N}_{fns} \\ &= \frac{2e}{h}\int d\varepsilon[f_{\mathcal{L}}(\varepsilon - eV) - f_{\mathcal{L}}(\varepsilon + eV)]\mathcal{T}^{A}_{fns}(\varepsilon) \\ &\quad + \frac{2e}{h}\int d\varepsilon[f_{\mathcal{L}}(\varepsilon - eV) - f_{\mathcal{R}}(\varepsilon)]\mathcal{T}^{N}_{fns}(\varepsilon), \quad (49)\end{aligned}$$

where

$$\begin{aligned}\mathcal{T}^{A}_{fns} &= \frac{1}{2}\sum_{i=1,3}\Big(\mathbf{\Gamma}^{\mathcal{L}f}(\varepsilon \mp eV)\breve{\mathbf{G}}^{r}_{c,c}(\varepsilon)\Big)_{ii+1} \Big(\mathbf{\Gamma}^{\mathcal{L}f}(\varepsilon \mp eV)\breve{\mathbf{G}}^{a}_{c,c}(\varepsilon)\Big)_{i+1i} \\ &= \frac{1}{2}\Big[\Gamma^{\mathcal{L}f}_{\uparrow}(\varepsilon - eV)\Gamma^{\mathcal{L}f}_{\downarrow}(\varepsilon + eV)|\breve{G}^{r}_{c,c;12}|^2 + \Gamma^{\mathcal{L}f}_{\downarrow}(\varepsilon - eV)\Gamma^{\mathcal{L}f}_{\uparrow}(\varepsilon + eV)|\breve{G}^{r}_{c,c;34}|^2\Big], \quad (50)\end{aligned}$$

$$\begin{aligned}\mathcal{T}^{N}_{fns} &= \frac{1}{2}\sum_{i=1,3}\Big(\mathbf{\Gamma}^{\mathcal{L}f}(\varepsilon \mp eV)\breve{\mathbf{G}}^{r}_{c,c}(\varepsilon)\mathbf{\Gamma}^{\mathcal{R}s}_{\rho}(\varepsilon)\breve{\mathbf{G}}^{a}_{c,c}(\varepsilon)\Big)_{ii} \\ &= \frac{1}{2}\rho^{\mathcal{R}s}(\varepsilon)\Gamma^{\mathcal{R}s}\Big\{\Gamma^{\mathcal{L}f}_{\uparrow}(\varepsilon - eV)\big[|\breve{G}^{r}_{c,c;11}|^2 + |\breve{G}^{r}_{c,c;21}|^2 \\ &\quad -2\frac{|\Delta_{\mathcal{R}}|}{\varepsilon}\mathrm{Re}\{\breve{G}^{r}_{c,c;11}\breve{G}^{a}_{c,c;21}\}\big] + \Gamma^{\mathcal{L}f}_{\downarrow}(\varepsilon - eV) \\ &\quad \big[|\breve{G}^{r}_{c,c;33}|^2 + |\breve{G}^{r}_{c,c;43}|^2 + 2\frac{|\Delta_{\mathcal{R}}|}{\varepsilon}\mathrm{Re}\{\breve{G}^{r}_{c,c;33}\breve{G}^{a}_{c,c;43}\}\big]\Big\}. \quad (51)\end{aligned}$$

The elements of the Green function matrix $\breve{G}^{r/a}_{c,c;11}$, $\breve{G}^{r/a}_{c,c;12}$,$\breve{G}^{r/a}_{c,c;21}$, $\breve{G}^{r/a}_{c,c;33}$, $\breve{G}^{r/a}_{c,c;34}$ and $\breve{G}^{r/a}_{c,c;43}$ are derived from Eq. (48) as

$$\breve{G}^{r}_{c,c;11} = \frac{(\sum_n \frac{1}{\varepsilon+\epsilon'_{n\downarrow}+i0^+})^{-1} + \frac{i}{2}\big[\Gamma^{\mathcal{L}f}_{\downarrow}(\varepsilon + eV) + \Gamma^{\mathcal{R}s}\varrho^{\mathcal{R}s}(\varepsilon)\big]}{\breve{G}_{fs1}(\varepsilon)}$$

$$\breve{G}^{r}_{c,c;12} = \breve{G}^{r}_{c,c;21} = \frac{\frac{i}{2}\Gamma^{\mathcal{R}s}\varrho^{\mathcal{R}s}(\varepsilon)\frac{|\Delta_{\mathcal{R}}|}{\varepsilon}}{\breve{G}_{fs1}(\varepsilon)},$$

$$\breve{G}^{r}_{c,c;33} = \frac{(\sum_n \frac{1}{\varepsilon+\epsilon'_{n\downarrow}+i0^+})^{-1} + \frac{i}{2}\big[\Gamma^{\mathcal{L}f}_{\uparrow}(\varepsilon + eV) + \Gamma^{\mathcal{R}s}\varrho^{\mathcal{R}s}(\varepsilon)\big]}{\breve{G}_{fs2}(\varepsilon)}$$

$$\breve{G}^{r}_{c,c;34} = \breve{G}^{r}_{c,c;43} = -\frac{\frac{i}{2}\Gamma^{\mathcal{R}s}\varrho^{\mathcal{R}s}(\varepsilon)\frac{|\Delta_{\mathcal{R}}|}{\varepsilon}}{\breve{G}_{fs2}(\varepsilon)},$$

in which

$$\begin{aligned}\breve{G}_{fs1}(\varepsilon) &= \Big\{\big(\sum_n \frac{1}{\varepsilon - \epsilon'_{n\uparrow} + i0^+}\big)^{-1} + \frac{i}{2}\big[\Gamma^{\mathcal{L}f}_{\uparrow}(\varepsilon - eV) \\ &\quad +\Gamma^{\mathcal{R}s}\varrho^{\mathcal{R}s}(\varepsilon)\big]\Big\}\Big\{\big(\sum_n \frac{1}{\varepsilon + \epsilon'_{n\downarrow} + i0^+}\big)^{-1} + \\ &\quad \frac{i}{2}\big[\Gamma^{\mathcal{L}f}_{\downarrow}(\varepsilon + eV) + \Gamma^{\mathcal{R}s}\varrho^{\mathcal{R}s}(\varepsilon)\big]\Big\} + \\ &\quad \frac{1}{4}\Big[\Gamma^{\mathcal{R}s}\varrho^{\mathcal{R}s}(\varepsilon)\frac{|\Delta_{\mathcal{R}}|}{\varepsilon}\Big]^2, \quad (52)\end{aligned}$$

$$\begin{aligned}\breve{G}_{fs2}(\varepsilon) &= \Big\{\big(\sum_n \frac{1}{\varepsilon - \epsilon'_{n\downarrow} + i0^+}\big)^{-1} + \frac{i}{2}\big[\Gamma^{\mathcal{L}f}_{\downarrow}(\varepsilon - eV) \\ &\quad +\Gamma^{\mathcal{R}s}\varrho^{\mathcal{R}s}(\varepsilon)\big]\Big\}\Big\{\big(\sum_n \frac{1}{\varepsilon + \epsilon'_{n\uparrow} + i0^+}\big)^{-1} + \\ &\quad \frac{i}{2}\big[\Gamma^{\mathcal{L}f}_{\uparrow}(\varepsilon + eV) + \Gamma^{\mathcal{R}s}\varrho^{\mathcal{R}s}(\varepsilon)\big]\Big\} + \\ &\quad \frac{1}{4}\Big[\Gamma^{\mathcal{R}s}\varrho^{\mathcal{R}s}(\varepsilon)\frac{|\Delta_{\mathcal{R}}|}{\varepsilon}\Big]^2. \quad (53)\end{aligned}$$

Compared to the work for the $N-QD-S$ system from the similar Keldysh formalism,[15] the derivation of the final current formula (49),(50) and (51) from the formalism we developed is more direct, simple and systematic. What we need to do is just some simple matrix algebra, while complicated mathematical techniques are needed in the derivation of the Green functions in the formalism of Sun et al..[15] Also the current formula permits us to investigate the I-V characteristics within a much wider bias voltage region in $F/I/N/I/S$ DBTSs.

The ferromagnetism and superconductor proximity are manifested in the dependence on the magnetization $h_{\mathcal{L}}$ and the magnitude of the superconducting order parameter $|\Delta_{\mathcal{R}}|$ of the full Green functions through self-energy matrices. From expressions (49,50,51), one observes that the current through a $F/I/N/I/S$ resonant structure results from different contributions.[13,55] $\mathcal{I}^{A}_{fns}$ is the Andreev reflection current: a spin-up/down electron/hole associated with spectral weight $\Gamma^{\mathcal{L}f}_{\uparrow}(\varepsilon - eV)/\Gamma^{\mathcal{L}f}_{\downarrow}(\varepsilon - eV)$ incident from the ferromagnetic lead is reflected as a spin-down/up hole/electron with spectral weight $\Gamma^{\mathcal{L}f}_{\downarrow}(\varepsilon + eV)/\ \Gamma^{\mathcal{L}f}_{\uparrow}(\varepsilon + eV)$ backward into the original lead, and at the same time two electrons in the normal region are removed into the superconductor as an electron pair with probability $|\breve{G}^{r}_{c,c;12}|^2/|\breve{G}^{r}_{c,c;34}|^2$. $\mathcal{I}^{N}_{fns}$ comes from three kinds of physical processes. The first and fourth terms in (51) represent the contribution from normal electron transmission, a spin-up/down electron/hole tunnels into the superconductor with probability $|\breve{G}^{r}_{c,c;11}|^2/|\breve{G}^{r}_{c,c;33}|^2$; the second and fifth terms describe the 'branch-crossing' process in the BTK theory,[55] a spin-up/down electron/hole in the ferromagnetic lead is converted into a spin-down/up hole/electron in the superconductor side, with particle pairs of opposite spins created in the normal region $|\breve{G}^{r}_{c,c;21}|^2/|\breve{G}^{r}_{c,c;43}|^2$. The terms left correspond to the net transfer of electrons/holes, along with the creation/annihilation of particle pairs inside the well and the annihilation/creation of pairs into the superconductor lead with probability proportional to $\mathrm{Re}\{\breve{G}^{r}_{c,c;11}\breve{G}^{a}_{c,c;21}\}/\mathrm{Re}\{\breve{G}^{r}_{c,c;33}\breve{G}^{a}_{c,c;43}\}$. At absolute zero temperature, the only contribution to the current is $\mathcal{I}^{A}_{fns}$ for $eV < |\Delta_{\mathcal{R}}|$, since in this case $\rho^{\mathcal{R}s}(\varepsilon)$ in $\mathcal{T}^{N}_{fns}$ becomes zero and then $I^{N}_{fns} = 0$. When $eV > |\Delta_{\mathcal{R}}|$

all processes contribute to the current. If one sets $h_{\mathcal{L}} = 0$ and assumes the wide-band approximation, the current formula will reduce to the result obtained by Sun et al[15] in the $N-QD-S$ case.

Assuming a single active level ε_0 in the well, we get the following linear-response conductance of the $F/I/N/I/S$ system

$$\mathcal{G}_{fns}(\varepsilon_0) = \frac{4e^2}{h}\frac{\Gamma_\uparrow^{\mathcal{L}f}\Gamma_\downarrow^{\mathcal{L}f}(\Gamma^{\mathcal{R}s})^2/4}{\Big[\varepsilon_0^2+\frac{\Gamma_\uparrow^{\mathcal{L}f}\Gamma_\downarrow^{\mathcal{L}f}+(\Gamma^{\mathcal{R}s})^2}{4}\Big]^2+\frac{\varepsilon_0^2(\Gamma_\uparrow^{\mathcal{L}f}-\Gamma_\downarrow^{\mathcal{L}f})^2}{4}} \tag{54}$$

For the completely polarized ferromagnetic lead, i.e., $h_{\mathcal{L}}/W = 1$, and $\Gamma_\downarrow^{\mathcal{L}f} = 0$, the linear conductance turns out to be zero, since there is no state available for the Andreev reflected spin-down holes. If the magnetization $h_{\mathcal{L}}$ is zero, $\Gamma_\uparrow^{\mathcal{L}f} = \Gamma_\downarrow^{\mathcal{L}f} = \Gamma^{\mathcal{L}}(0)$, the ferromagnetic lead becomes a normal metal, and the conductance is reduced to

$$\mathcal{G}_{nns}(\varepsilon_0) = \frac{4e^2}{h}\Big(\frac{2\Gamma^{\mathcal{L}}(0)\Gamma^{\mathcal{R}s}}{4\varepsilon_0^2+[\Gamma^{\mathcal{L}}(0)]^2+(\Gamma^{\mathcal{R}s})^2}\Big)^2, \tag{55}$$

which is the same as the result obtained by Beenakker from the scattering matrix approach.[56] In contrast to a single F/S junction,[36] the conductance of an $N/I/N/I/S$ resonant structure is always not less than that of the $F/I/N/I/S$ structure, regardless of the value of the magnetization $h_{\mathcal{L}}$. At $\varepsilon_0 = 0$ the conductance in the $N/I/N/I/S$ structure is maximal for symmetric couplings $\Gamma^{\mathcal{L}}(0) = \Gamma^{\mathcal{R}s}$, equaling to $4e^2/h$ twice that in the $N/I/N/I/N$ case. Moreover the line shapes of the linear-response conductances (54) and (55) which decay as ε_0^{-4} are not of the simple Lorentzian form $\Gamma^{\mathcal{L}}\Gamma^{\mathcal{R}}/[\varepsilon_0^2+(\Gamma^{\mathcal{L}}+\Gamma^{\mathcal{R}})^2/4]$.

Let us analyze further the spin polarization dependence of $\mathcal{G}_{fns}$ at resonance $\varepsilon_0 = 0$ for different couplings. Setting $\Gamma^{\mathcal{R}s} = \lambda\Gamma^{\mathcal{L}f}(0)$, Eq. (54) evolves into

$$\mathcal{G}_{fns} = \frac{4e^2}{h}\frac{4\kappa\lambda^2}{(\kappa+\lambda^2)^2}, \tag{56}$$

where $\kappa = \sqrt{1-h_{\mathcal{L}}^2/W^2}$ is a quantity characterizing the degree of spin polarization of the ferromagnetic lead: $\kappa = 1$ for normal metals and $\kappa = 0$ for completely polarized ferromagnets. When $\lambda \geq 1$, the conductance increases with increasing κ, implying that the conductance decreases when the degree of spin polarization rises. If $\lambda < 1$, the conductance first increases with increasing the spin polarization and then decreases rapidly after it reaches its maximum value $4e^2/h$. The critical value of κ is given by $\kappa = \lambda^2$. This interesting result is also obtained by Zhu et al.,[17] shown in Fig. 2 of their paper.

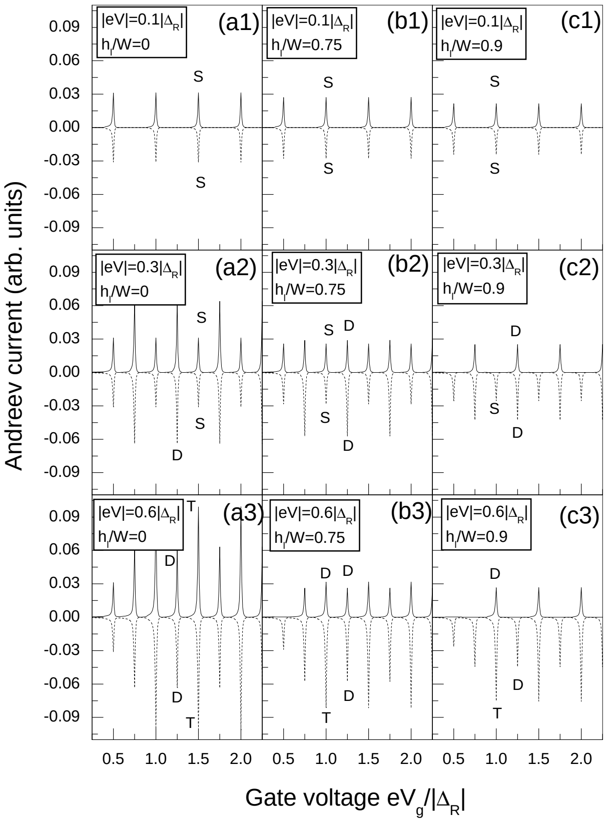

FIG. 6: The Andreev current spectra at zero temperature and fixed bias voltage for different spin polarizations (a) $h_{\mathcal{L}}/W = 0$, (b) $h_{\mathcal{L}}/W = 0.75$ and (c) $h_{\mathcal{L}}/W = 0.9$, where $W = 2|\Delta_{\mathcal{R}}|$. The full lines correspond to the results when $eV > 0$ and the dashed when $eV < 0$. Labels S, D and T are used to denote the current peaks arising from the resonant Andreev reflections involving single, double or triple levels, respectively. Here we assume 20 levels with identical level separation $0.5|\Delta_{\mathcal{R}}|$, and the first level aligns with the chemical potential of the superconductor lead when $V_g = 0$. The other parameters are $\Gamma^{\mathcal{L}f}(0) = \Gamma^{\mathcal{R}s} = 0.01|\Delta_{\mathcal{R}}|$.

Next we explore the dependence of the Andreev current spectrum on the degree of spin polarization of the ferromagnetic lead. From the schematic view of the resonant Andreev reflection processes in $F/I/N/I/S$ structures, one immediately becomes aware that the resonant Andreev current is determined mainly by the applied bias voltage V, the ratio of the strength of ferromagnetic magnetization to the bandwidth $h_{\mathcal{L}}/W$, and the level separation $\delta\varepsilon_n$. We choose a special level separation $\Delta\varepsilon_n = 0.501|\Delta_{\mathcal{R}}|$, a case in which at most three levels are allowed to fall into the energy gap of the superconductor lead. For simplicity we assume identical level separations and do not consider the influence of the bias voltage on the level shift for convenience of comparison. At fixed bias voltage smaller than the energy gap $|\Delta_{\mathcal{R}}|$, *resonant Andreev reflection takes place whenever the chemical potential of the superconductor lies just in between two levels and there are states available for the* *reflected electrons/holes.* The energy levels $\epsilon_n - eV_g$ can be shifted up and down by tuning continuously the gate voltage V_g. Therefore, one can expects a series of peaks in the Andreev current as a function of V_g.

In Fig. 6 we present numerical results of the Andreev current as a function of the gate voltage eV_g for different spin polarizations $h_{\mathcal{L}}/W$ and different bias voltages eV. The cases of positive and negative bias voltage are considered to compare the Andreev current contributed from electron and hole transmission. Let us first inspect the Andreev current spectra in the $N/I/N/I/S$ case (Fig. 6(a1)-(6a3)).[15] At a small positive bias voltage $eV = 0.1|\Delta_{\mathcal{R}}|$(Fig. 6(a1)), a series of peaks labelled by S with the same separation as the level spacing is observed. These peaks come from the resonant Andreev reflection processes by electron tunneling through a single level aligned with the chemical potential of the superconductor. When the bias voltage is small, there is no possibility for two levels to satisfy the resonant Andreev reflection condition. As the bias increases to $eV = 0.3|\Delta_{\mathcal{R}}|$ (Fig. 6(a2)), there is possibility for two neighboring levels to lie equally above and below the chemical potential of the superconductor. The condition of the resonant Andreev reflection involving two levels can be satisfied and two-level Andreev reflection also contributes to the Andreev current. As a result another series of resonant Andreev current peaks labelled by D is observed neighboring to the original series from single level contributions. These D peaks, with the same spacing as the S series and $0.25|\Delta_{\mathcal{R}}|$ away from it, stand out for their double height compared to the S ones. This is because for the D peaks two neighboring levels are involved in the corresponding resonant Andreev reflection processes, so the probability is doubled as compared to the single level situation. At a still higher bias voltage $eV = 0.6|\Delta_{\mathcal{R}}|$ (Fig. 6(a3)) the Andreev current spectrum can be understood similarly, the S-type peaks are now replaced by T ones with tripled amplitudes, resulting from three-level contributions. Since at $eV = 0.6|\Delta_{\mathcal{R}}|$, two additional levels near the middle one in alignment with the chemical potential also contribute to the Andreev current, so there are three neighboring levels taking part in resonant Andreev reflections, making the height of the T series three times as that of the S ones. When the bias is reversed, the Andreev current becomes negative, implying that the Andreev reflection is induced by hole transmission. However, the Andreev current spectra remains unchanged. Since in normal metals the DOS is spin degenerate, complete resonant Andreev reflections are guaranteed for electrons as well as their hole counterparts. Therefore, except for the sign the Andreev current spectra are the same for electron ($V > 0$) and hole transmission ($V < 0$). The above phenomena can also be understood from the intuitive diagrams in Fig. 7, with different spin-up and spin-down bands of the ferromagnets replaced by identical ones of the normal metals.

In a $F/I/N/I/S$ resonant structure the Andreev current depends not only on the position of the quantum well levels as in the normal case, but also on whether there are available states for the backward reflecting holes. The Andreev spectra for electron and hole transmission appear to be different if the ferromagnetic lead is of large spin polarization. For the completely polarized ferromagnetic lead, no Andreev current is expected due to the absence of empty states for the returning holes. We therefore choose the spin polarizations $h_{\mathcal{L}}/W = 0.75$ and $h_{\mathcal{L}}/W = 0.9$ for our purpose, where $W = 2|\Delta_{\mathcal{R}}|$, and the results are given in Fig. 6 (b1-b3) and (c1-c3). At a low bias voltage $eV = 0.1|\Delta_{\mathcal{R}}|$ there are still available states for the reflecting holes and the Andreev current exhibits the same resonant spectrum as in the normal

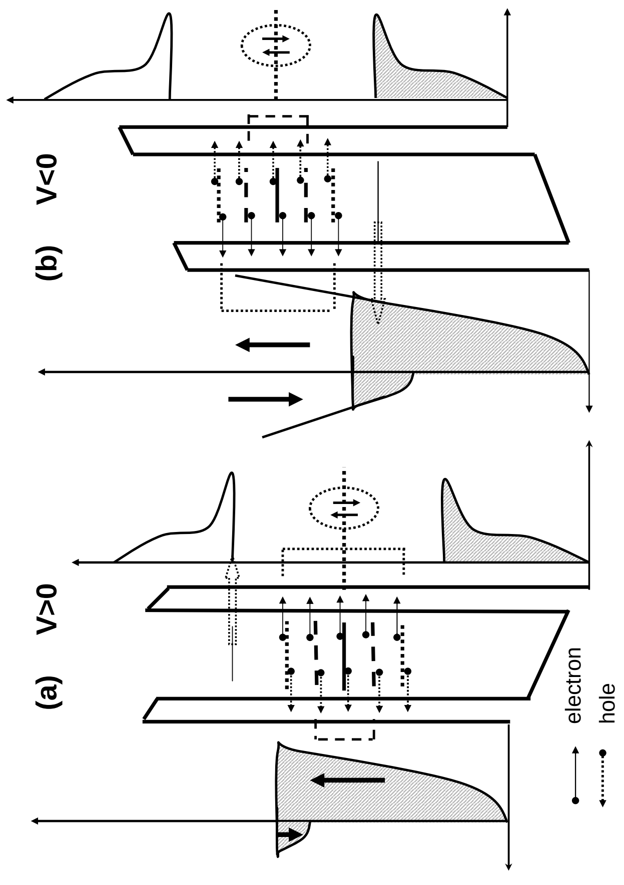

FIG. 7: Schematic views of the resonant Andreev reflection processes arising from the electron (a) and hole (b) transmission from the ferromagnetic lead. The hatched region represents states that are occupied by electrons. The Andreev current peaks labelled by S in Fig. 6 is originated from the Andreev reflection process involving a *single* level represented by the solid line, D *double* levels by dashed lines and T *triple* levels by dotted lines. The block arrows stand for the process at the edges of the superconducting band involving electron tunneling through the level located at $\varepsilon_n = |\Delta_{\mathcal{R}}|$, which results in sharp peaks in the I-V characteristics.

case, with slightly suppressed peak amplitude. If the bias voltage is $eV = 0.3|\Delta_{\mathcal{R}}|$, the spin-down band of polarization $h_{\mathcal{L}}/W = 0.9$ moves above the chemical potential of the superconducting lead, leaving only the possibility for a spin-up electron to be transmitted through a level below the chemical potential and then reflected backwards through the neighboring level above the chemical potential to the spin-down band. Hence we can only observe the D-type peaks with amplitude half that in the normal case in the spectrum (Fig. 6(c2)). As $h_{\mathcal{L}}/W = 0.75$, the D-type Andreev current peaks with half the amplitude of the normal case are originated from the same resonant Andreev reflection processes by spin-up electrons going through the states below the chemical potential as in the case $h_{\mathcal{L}}/W = 0.9$. This is the reason why we observe the amplitudes of the S and D-type peaks to be nearly the same (Fig. 6(b2)). As the bias voltage eV is further increased to $0.6|\Delta_{\mathcal{R}}|$, the spin-down bands for $h_{\mathcal{L}}/W = 0.75$ and $h_{\mathcal{L}}/W = 0.9$ shift above the chemical potential of the superconductor, and one can no longer observe the series of S-type peaks from the contribution of the levels just at the chemical potential. For ferromagnets with high spin polarization, the current arises only from the resonant Andreev reflections by the spin-up electrons tunneling through the levels $0.5|\Delta_{\mathcal{R}}|$ below the chemical potential. Thus the Andreev current spectrum ((Fig. 6(c3)) only consists of a series of peaks at the positions of the T-type peaks in the normal case. Whereas in the small polarization case ((Fig. 6(b3)), the Andreev reflections involving two neighboring levels and two of three levels contributing to the T-type peaks in the normal case can happen, and a series of resonant peaks with equal separation $0.25|\Delta_{\mathcal{R}}|$ is observed.

Schematic views of the above resonant Andreev reflection processes for electron transmission are given in Fig. 7(a). When the bias voltage is reversed, the current is contributed from hole transmissions, and the situation is now very similar to the normal case. The only difference is that the amplitudes of the peaks in the ferromagnetic case are suppressed due to the reduced DOS for the reflected electrons. The relation among the S-, D- and T-type current amplitudes still hold, for which a heuristic physical picture is given in the Fig. 7(b). When the level spacings are not identical, more interesting and complicated resonant Andreev current patterns can be expected.[15] However, we can still appreciate and analyze them from the intuitive pictures of Fig. 7 whatever the Andreev current spectra may be.

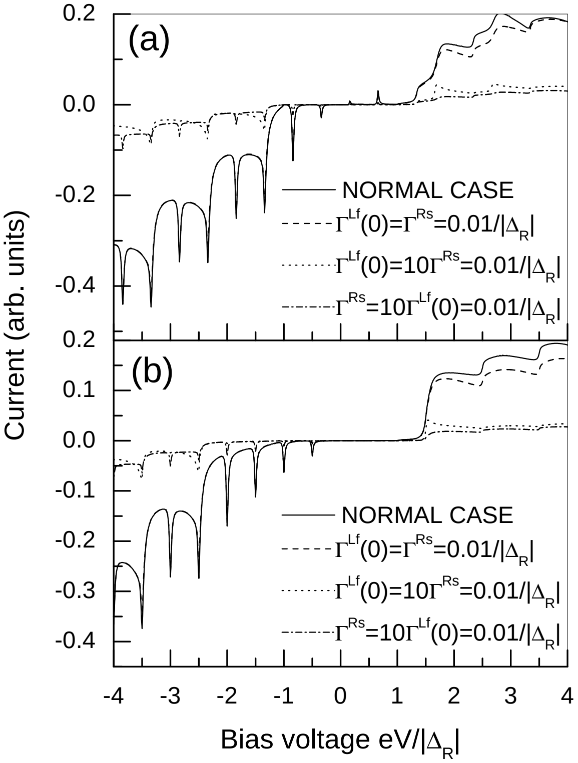

FIG. 8: I-V characteristics of a $F/I/N/I/S$ resonant structure at temperature $0.1|\Delta_{\mathcal{R}}|$ for small level spacing $\Delta\varepsilon_n =$ (a) $0.33|\Delta_{\mathcal{R}}|$ below and (b) $0.25|\Delta_{\mathcal{R}}|$ above the chemical potential of the superconducting lead when $V = 0$. The solid curves are the results for the $N/I/N/I/S$ case with symmetric coupling $\Gamma^{\mathcal{L}f}(0) = \Gamma^{\mathcal{R}s} = 0.01|\Delta_{\mathcal{R}}|$, and the other curves for the $F/I/N/I/S$ structure with $h_{\mathcal{L}}/W = 0.5$.

The I-V characteristics of this kind of generic hybrid structure is also interesting. It is known that the resonant Andreev reflection process also contributes to the current when the bias voltage eV is greater than $|\Delta_{\mathcal{R}}|$, the energy gap of the superconducting lead. For this reason we consider cases in which the level spacing $\Delta\varepsilon_n$ can be either smaller or greater than the energy gap $|\Delta_{\mathcal{R}}|$, as well as when the first level ε_0 is either below or above the chemical potential of the superconductor when $V = 0$. Fig. (8a) and (8b) give the I-V curves for small level spacing $\Delta\varepsilon_n = 0.5|\Delta_{\mathcal{R}}|$ when the first level $\varepsilon_0 = -0.33|\Delta_{\mathcal{R}}|$ lies below (Fig. 8a) and $\varepsilon_0 = 0.25|\Delta_{\mathcal{R}}|$ above (Fig. 8b) the chemical potential of the superconductor lead. As usual we approximate the variation of the energy levels with the bias voltage by $\varepsilon_n + 0.5eV$. There is no substantial difference between the I-V characteristics of the $F/I/N/I/S$ and $N/I/N/I/S$ systems when the level separation is small, as shown by the full and dashed lines in Fig. 8. However, the current as a function of the bias voltage is strongly dependent on the symmetry between the couplings and the level configuration, especially when the applied bias is positive. The peaks in the I-V curves are originated from the resonant Andreev reflections, which emerge at some specific bias voltages when the resonant Andreev reflection condition is satisfied. The irregular current plateaus come from the normal particle transmission. There are two types of current plateaus with different heights. Those with higher height are determined by particle tunneling through the level aligned with one of the edges of the superconducting

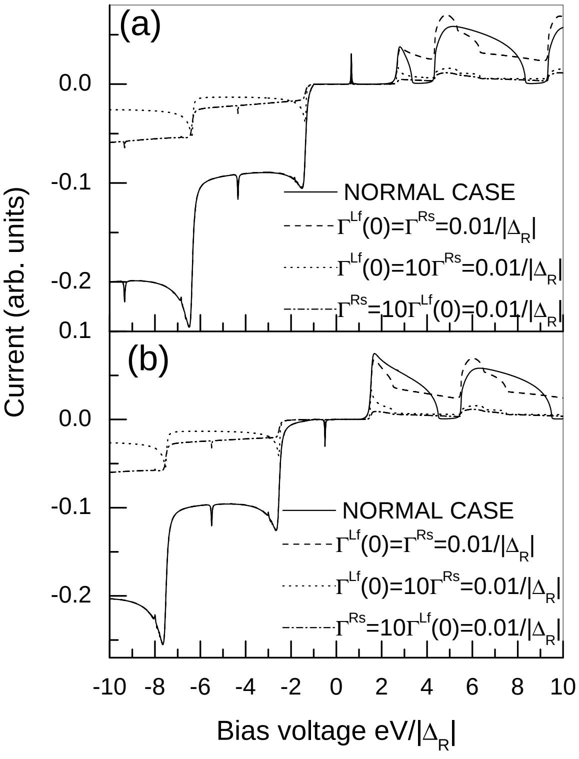

FIG. 9: Same as Fig. 8, but for level spacing $\Delta\varepsilon_n = 2.5|\Delta_{\mathcal{R}}| > W = 2|\Delta_{\mathcal{R}}|$ when the first level ε_0 lies (a) $0.33|\Delta_{\mathcal{R}}|$ below and (b) $0.25|\Delta_{\mathcal{R}}|$ above the chemical potential of the superconducting lead when $V = 0$.

energy gap at which the DOS is divergent, represented by a block arrow in Fig. 7, while the others are contributed from the levels away from the edges. Such an analysis can be confirmed by the following simple estimation: If $\varepsilon_0 = -0.33|\Delta_{\mathcal{R}}|$, then at bias $-0.33|\Delta_{\mathcal{R}}| + 0.5eV = 0$ and $0.17|\Delta_{\mathcal{R}}| + 0.5eV = 0$, the resonant Andreev reflection condition is satisfied and current peaks emerge at $eV = 0.66|\Delta_{\mathcal{R}}|$ and $eV = -0.34|\Delta_{\mathcal{R}}|$. For the first plateau to appear, we need $\varepsilon_n + 0.5eV = \pm|\Delta_{\mathcal{R}}|$ and $eV \geq \pm|\Delta_{\mathcal{R}}|$, i.e., $eV = 1.66|\Delta_{\mathcal{R}}|$ and $eV = -1.34|\Delta_{\mathcal{R}}|$. The numerical results are consistent with this simple argument (Fig. 8(a)).

In the case of negative bias $eV < -|\Delta_{\mathcal{R}}|$, the levels are pushed down gradually inside the energy gap and the resonant Andreev reflection condition is eventually satisfied at some bias voltages. Since both the normal particle tunneling and the resonant Andreev reflection contribute to the current, one observes a series of equally spaced resonant peaks superimposed onto the plateaus with identical widths. When the couplings become asymmetric (one of the couplings is weakened), both the Andreev current peaks and current plateaus are suppressed. This is because the normal and Andreev current is proportional to the product of the couplings $\Gamma^{\mathcal{L}f}(0)\Gamma^{\mathcal{R}s}$, as can be found in the formulae (49), (50) and (51). It has already been found analytically by Sun et al[15] that the Andreev reflection probability is maximized for symmetric couplings in $N-QD-S$ structures and decreases rapidly with the increasing coupling asymmetry. In the special asymmetric coupling case where $\Gamma^{\mathcal{R}s} << \Gamma^{\mathcal{L}f}(0)$, the sharp DOS at the edges of the superconductor energy gap can be discerned clearly whenever particles transmit through a level aligned to the edge (see the dotted lines in Fig. 8). This can be easily understood from the Breit-Wigner formula for resonant normal electron transmission at resonance $\mathcal{T} = 4\Gamma^{\mathcal{L}f}(0)\Gamma^{\mathcal{R}s}\rho^{\mathcal{L}f}\rho^{\mathcal{R}s}/[\Gamma^{\mathcal{L}f}(0)\rho^{\mathcal{L}f} + \Gamma^{\mathcal{R}s}\rho^{\mathcal{R}s}]^2$. The transmission probability $\mathcal{T}$ depends on the ratio between the level-widths $\Gamma^{\mathcal{L}f}(0)\rho^{\mathcal{L}f}$ and $\Gamma^{\mathcal{R}s}\rho^{\mathcal{R}s}$. At the edges of the gap, $\rho^{\mathcal{R}s}$ is divergent and thus the coupling constant should be small enough to balance these two level-widths to guarantee high transmission. Notice that the ferromagnetic feature can not be observed in the I-V curves of $F/I/N/I/S$ structures when the level spacing is small. It can only be displayed when the level separation is greater than the band-width of the ferromagnets. In Fig. 9 we present the results of I-V relation of this case for different couplings and different level arrangements. As expected, the degree of spin polarization of the ferromagnetic lead is reflected in the I-V curves. In the normal case and when $eV > 0$, the current first develops a resonant Andreev peak at $-0.33|\Delta_{\mathcal{R}}| + 0.5eV = 0$ and exhibits usual resonant peaks in the double-barrier structure after a narrow peak with width determined from $-0.33|\Delta_{\mathcal{R}}| + 0.5eV = |\Delta_{\mathcal{R}}|$ and $-0.33|\Delta_{\mathcal{R}}| + 0.5eV = eV - W$. When the bias is reversed, the current displays a plateau from the position $-0.33|\Delta_{\mathcal{R}}| + 0.5eV = -|\Delta_{\mathcal{R}}|$, superimposed by some weak Andreev peaks arising from the resonant Andreev reflections for $|\varepsilon| > |\Delta_{\mathcal{R}}|$. If $\varepsilon_0 = 0.25|\Delta_{\mathcal{R}}|$ when $V = 0$, one observes an I-V characteristics similar to that of a usual magnetic DBTS in the case of positive bias $V > 0$, and in the negative bias case a resonant Andreev peak at $0.25 + 0.5eV = 0$ and a plateau-peak structure similar to the case $\varepsilon_0 = -0.33|\Delta_{\mathcal{R}}|$. For $F/I/N/I/S$ structures, the current develops both a resonant peak as well as a shoulder which are more prominent in the high bias case for $eV > 0$, while they keep nearly the same as in the $N/I/N/I/S$ structure when the bias is negative. This picture is violated when the couplings become asymmetric. As in the case of small level spacing, the sharp DOS at the edges of the energy gap is also prominent in the I-V characteristics when the coupling to the superconductor side $\Gamma^{\mathcal{R}s}$ is much smaller than that to the ferromagnetic side $\Gamma^{\mathcal{L}f}(0)$. The spin polarization of the ferromagnet can thus be measured when the couplings to the ferromagnetic and superconducting leads are symmetric, as suggested from the comparison of the dashed, dotted and dash-dotted lines in Fig. 9. It is noted that the I-V characteristics of $F/I/N/I/S$ resonant structures are qualitatively right, because the idea about the bandwidth of the superconductor is somewhat vague within its semiconductor model.[31]

In summary, we have investigated in this subsection the Andreev current spectra and I-V relations of a $F/I/N/I/S$ resonant structure in detail. Interesting dependence on the ferromagnetic spin polarization of the linear conductance is discussed in terms of analytic expressions, given by Eqs. (54) and (56). Our results demonstrate that the peak structure of the Andreev current as a function of the gate voltage is determined by the applied bias (both the value and sign) and the degree of spin polarization, which differs substantially from the results under the wide-band approximation. The I-V characteristics, closely associated with the level arrangement, coupling symmetry, bias sign and spin polarization, can be employed to characterize the density of states (DOS) of both ferromagnets and superconductors by tuning the coupling strengths.

C. S/I/N/I/S structures

The discovery of the Josephson effect[59] has provoked a lasting research interest in the properties of the DC-and AC-Josephson current in mesoscopic $S/N/S$ junctions in thirty years.[31,60] When the width of the normal region is smaller than the coherence length, electron pairs can coherently tunnel from one superconductor to the other, inducing a phase-dependent DC current even when the bias is zero. Early in 1963, Ambergaokar and Baratoff[61] derived a useful formula for the supercurrent in $S/I/S$ junctions with the help of the Gor'kov Green functions. In the 1990's investigations on the mesoscopic $S/N/S$ junctions became timely[60] due to the advances in experimental techniques. In most of these work, the scattering matrix method based on the Bogoliuboiv-de Gennes (BdG) equation[62] is commonly used. In a $S/N/S$ junction, the Andreev reflections at the N/S boundaries confined the quasi-particle inside the normal region, resulting in the bound states sensitive to the superconducting phase difference of the two superconductors.[32] Impurities inside the normal region altering the quasi-particle wave interference,[33] and the asymmetry between the two energy gaps can also modify the Josephson current.[63] Glazman and Matreev,[64] and Ishizaka et al.[65] have studied the influence of the Coulomb interactions on the Josephson current in $S-QD-S$ systems. Research were also conducted on the DC Josephson current in noninteracting symmetric $S-QD-S$ structures by Beenakker using the scattering matrix approach,[66] and by Lin's Group from the Keldysh NEGF method.[67] However, these investigations are restricted to the symmetric case-the same couplings and energy gaps. Motivated by this limitation, we investigate in this subsection the DC Josephson current through a general $S/I/N/I/S$ resonant structure, in order to reveal the dependence of the Josephson current on the energy gaps. Results for the AC Josephson current will be reported elsewhere.

Neglecting the interaction effects in the central region we obtain an unexpectedly simple form of the DC Josephson current formula for a general $S/I/N/I/S$ system from Eq. (35)

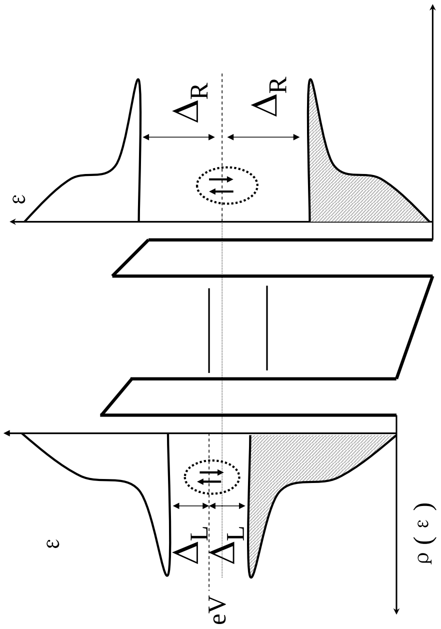

FIG. 10: A schematic potential profile for a biased DBTS attached to two superconducting leads with order parameters $\Delta_\mathcal{L}$ and $\Delta_\mathcal{R}$. Here the hatched region represent occupied electron states.

$$\begin{aligned}
\mathcal{I}_{sns}(\varphi_s) &= \frac{e}{2h}\sum^{i=1,3}\int d\varepsilon \mathrm{Im}\Big\{f(\varepsilon)\Big(\big[\tilde{\mathbf{\Gamma}}^{\mathcal{L}s}_{\varrho}(\varepsilon)-\mathbf{\Gamma}^{\mathcal{R}s}_{\varrho}(\varepsilon)\big] \\
&\qquad \widetilde{\mathbf{G}}^{r}_{c,c}(\varepsilon)+\big[\tilde{\mathbf{\Gamma}}^{\mathcal{L}s}_{\varrho^*}(\varepsilon)-\mathbf{\Gamma}^{\mathcal{R}s}_{\varrho^*}(\varepsilon)\big]\widetilde{\mathbf{G}}^{a}_{c,c}(\varepsilon)\Big)_{ii}\Big\}, \\
&= -\frac{2e}{h}\sin\varphi_s\int_{-\infty}^{+\infty} d\varepsilon\Gamma^{\mathcal{L}s}\Gamma^{\mathcal{R}s}|\Delta_\mathcal{L}\Delta_\mathcal{R}|\frac{f(\varepsilon)}{\varepsilon^2} \\
&\qquad \mathrm{Im}\{\frac{\varrho^{\mathcal{L}s}\varrho^{\mathcal{R}s}}{\widetilde{G}^r_s}\} \\
&= -\frac{e}{\hbar}\sin\varphi_s\sum_{0<\varepsilon_p<|\Delta_\mathcal{L}|}\tanh(\varepsilon_p/2k_BT) \\
&\qquad \lim_{\varepsilon\to\varepsilon_p}\frac{(\varepsilon-\varepsilon_p)\Gamma^{\mathcal{L}s}\Gamma^{\mathcal{R}s}|\Delta_\mathcal{L}\Delta_\mathcal{R}|}{\sqrt{(|\Delta_\mathcal{L}|^2-\varepsilon^2)(|\Delta_\mathcal{R}|^2-\varepsilon^2)}\widetilde{G}^r_s(\varepsilon)} \\
&\qquad -\frac{2e}{h}\sin\varphi_s\Big[\overbrace{\int_{-|\Delta_\mathcal{R}|}^{-|\Delta_\mathcal{L}|}+\int_{|\Delta_\mathcal{L}|}^{|\Delta_\mathcal{R}|}}^{2}+
\end{aligned}$$

$$\overbrace{\int_{-\infty}^{-|\Delta_{\mathcal{R}}|}+\int_{|\Delta_{\mathcal{R}}|}^{+\infty}}^{3}\Big]\Gamma^{\mathcal{L}s}\Gamma^{\mathcal{R}s}|\Delta_{\mathcal{L}}\Delta_{\mathcal{R}}| \frac{f(\varepsilon)}{\varepsilon^2}\mathrm{Im}\Big\{\frac{\varrho^{\mathcal{L}s}\varrho^{\mathcal{R}s}}{\widetilde{G}^r_s}\Big\}d\varepsilon$$

$$= \mathcal{I}_1+\mathcal{I}_2+\mathcal{I}_3, \tag{57}$$

where we assume in general $|\Delta_{\mathcal{L}}| \leq |\Delta_{\mathcal{R}}|$, and ε_p, the energies of the discrete Andreev bound states, are the poles of the spectral function $\widetilde{G}^r_s(\varepsilon)$

$$\widetilde{G}^r_s(\varepsilon) = \Big\{\Big(\sum_n \frac{1}{\varepsilon-\epsilon'_n+i0^+}\Big)^{-1}+\frac{i}{2}\big[\Gamma^{\mathcal{L}s}\varrho^{\mathcal{L}s}(\varepsilon) +\Gamma^{\mathcal{R}s}\varrho^{\mathcal{R}s}(\varepsilon)\big]\Big\}\Big\{\Big(\sum_n \frac{1}{\varepsilon+\epsilon'_n+i0^+}\Big)^{-1}+ \frac{i}{2}\big[\Gamma^{\mathcal{L}s}\varrho^{\mathcal{L}s}(\varepsilon)+\Gamma^{\mathcal{R}s}\varrho^{\mathcal{R}s}(\varepsilon)\big]\Big\}+\frac{1}{4}\Big[\frac{(\Gamma^{\mathcal{L}s}|\Delta_{\mathcal{L}}|)^2}{\varepsilon^2-|\Delta_{\mathcal{L}}|^2} +\frac{(\Gamma^{\mathcal{R}s}|\Delta_{\mathcal{R}}|)^2}{\varepsilon^2-|\Delta_{\mathcal{R}}|^2}+2\cos\varphi_s\Gamma^{\mathcal{L}s}\Gamma^{\mathcal{R}s}\frac{|\Delta_{\mathcal{L}}\Delta_{\mathcal{R}}|}{\varepsilon^2} \varrho^{\mathcal{L}s}(\varepsilon)\varrho^{\mathcal{R}s}(\varepsilon)\Big]. \tag{58}$$

It is seen from Eq. (57) that the DC Josephson current $\mathcal{I}_{sns}$ in a general $S/I/N/I/S$ system has contributions from three different scattering processes: $\mathcal{I}_1$ results from the resonant Josephson tunneling through the discrete Andreev bound states given by $\widetilde{G}^r_s(\varepsilon)=0$ within $|\varepsilon|<|\Delta_{\mathcal{L}}|$; $\mathcal{I}_2$ from the quasi-particle escaping through broadened levels from the normal region to the weaker superconductor side, i.e., $|\Delta_{\mathcal{L}}|\leq|\varepsilon|<|\Delta_{\mathcal{R}}|$; and $\mathcal{I}_3$ from quasi-particle tunneling from the normal region to both superconductors $|\varepsilon|\geq|\Delta_{\mathcal{R}}|$.[63] One can consider Eq. (57) as an extension to the asymmetric case of the Beenakker's result for symmetric $S-QD-S$ systems.[66,68] In addition one can check after simple algebra that the DC Josephson current formula (57) for the general asymmetric $S/I/N/I/S$ system reduces to the known result for the symmetric case.[66,67,68]

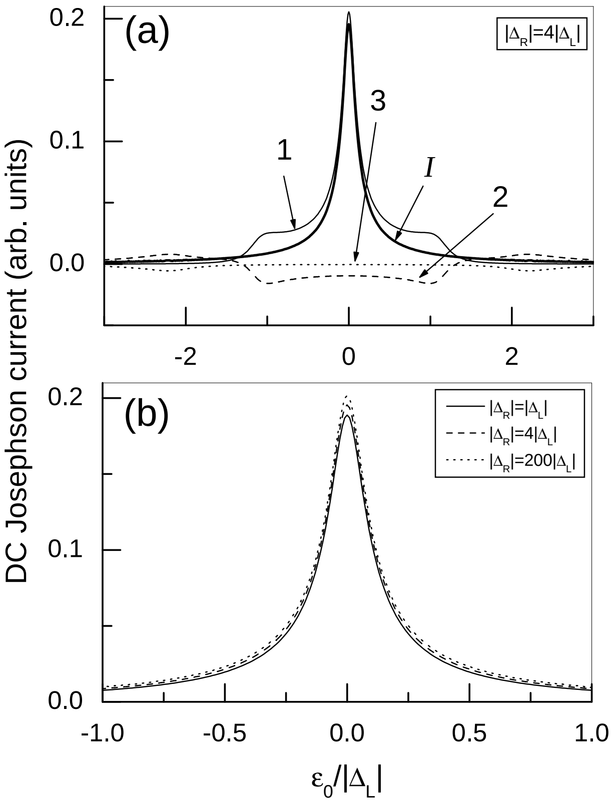

FIG. 11: The DC Josephson current vs ε_0 for (a) different scattering processes, and (b) different energy gaps, where we take symmetric couplings as $\Gamma^{\mathcal{L}s}=\Gamma^{\mathcal{R}s}=0.01|\Delta_{\mathcal{L}}|$. The superconducting phase difference is $\varphi_s=\pi/2$.

Now we consider the simplest situation in which there is only a single active level ε_0 in the central normal region. It is expected that the resonant Josephson scattering via the Andreev bound states ε_p will dominate the DC Josephson current. In Fig. 11 we plot this quantity at zero temperature, calculated from Eq. (57) as a function of the single level energy ε_0 for symmetric couplings $\Gamma^{\mathcal{L}s}=\Gamma^{\mathcal{R}s}=0.01|\Delta_{\mathcal{L}}|$. However, the superconducting energy gaps are allowed to be asymmetric. The superconducting phase difference is chosen as$\varphi_s=\pi/2$. The total current labelled by I in Fig. 11(a) has a resonant peak when the single level is aligned with the chemical potential of the superconductor, i.e., $\varepsilon_0=0$, resulting from the constructive interference between the forward Andreev state $+\varepsilon_p$ and backward Andreev state $-\varepsilon_p$. Inspecting the current components for three different scattering regions $|\varepsilon|<|\Delta_{\mathcal{L}}|$, $|\Delta_{\mathcal{L}}|\leq|\varepsilon|<|\Delta_{\mathcal{R}}|$ and $|\varepsilon|\geq|\Delta_{\mathcal{R}}|$,[63] labelled respectively by 1, 2 and 3, one finds that the current component 1 contributed by discrete Andreev levels makes the major contribution to the DC Josephson current. It possesses one peak at $\varepsilon_0=0$ plus two side peaks pinned at $\varepsilon_0=\pm|\Delta_{\mathcal{L}}|$ which are offset by two peaks in the current component $\mathcal{I}_2$, in which two additional wider side peaks cancelled exactly by $\mathcal{I}_3$. The side peaks come from the abnormal superconductor DOS singularities at the edges of the energy gap(s), and the exact cancellation of these side peaks in the total Josephson current is due to the fact that both electron-like and hole-like excitations can escape through the active level from the superconductor to the central normal region. This is equivalent, mathematically, to the vanishing residues of the spectral function $\widetilde{G}^r_s$.[67] In contrast to the symmetric case $|\Delta_{\mathcal{L}}|=|\Delta_{\mathcal{R}}|$, the DC Josephson current is slightly enhanced in the asymmetric case $|\Delta_{\mathcal{L}}|<|\Delta_{\mathcal{R}}|$, as demonstrated in Fig. 11(b). This result differs from the usual $S/N/S$ structure, where the current is greatly enhanced.[63] The reason is that the energy levels lie within $|\varepsilon|<|\Delta_{\mathcal{L}}|$, and then resonant Josephson tunneling dominates the DC current, as can be seen more clearly in the current-phase relation in Fig. 12. The significant enhancement of the DC Josephson current may be observed in a resonant $S/I/N/I/S$ system with many lev-

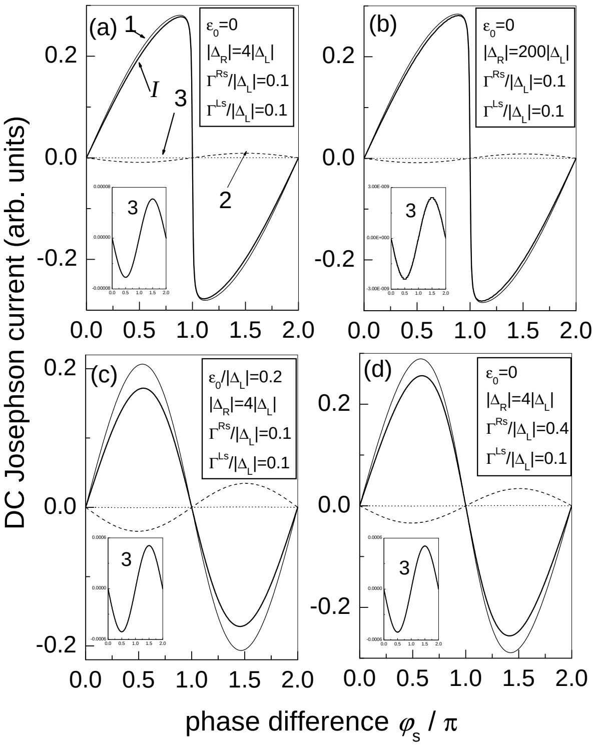

FIG. 12: The current-phase relation for a resonant $S/I/N/I/S$ structure, where the insets are enlargements of the current component $\mathcal{I}_3$. Here the total DC Josephson current $\mathcal{I}_{sns}$ and its components $\mathcal{I}_1$, $\mathcal{I}_2$ and $\mathcal{I}_3$ are represented by the thick solid, thin solid, dashed and dotted lines, respectively.

els located inside the region $|\varepsilon| < |\Delta_{\mathcal{L}}|$, since in this case so many levels are active to contribute to the Josephson current. Fig.12 shows the resonant DC Josephson current at zero temperature as a function of the superconducting phase difference φ_s for general asymmetric $S/I/N/I/S$ systems. When $\varepsilon_0 = 0$, i.e. the single level is exactly located at the position of the superconducting chemical potential, the DC Josephson current $\mathcal{I}_{sns}(\varphi_s)$ and its component $\mathcal{I}_1$ vs the superconducting phase difference φ_s is of the sawtooth shape (Fig. 12 (a) and (b)), no matter how big the difference between the two superconducting energy gaps is. The physical origin of the sharp discontinuity at $\varphi_s = \pi$ is the same as in the usual $S/N/S$ junction:[33,69] the Andreev levels ε_p and $-\varepsilon_p$ determined from the spectral function $\widetilde{G}^r_s(\varepsilon) = 0$ at $\varphi_s = 0$ interchange their position at $\varphi_s = \pi$, producing a discontinuity in the DC Josephson current. Unlike the usual $S/N/S$ structure, the supercurrent-phase relation has a weak dependence on the asymmetry between the superconducting energy gaps in resonant $S/I/N/I/S$ structures. This is because the main contribution to the DC Josephson current in resonant structures with a single level is mainly from the Andreev refection processes inside the region $|\varepsilon| < |\Delta_{\mathcal{L}}|$, where the energy of the Andreev bound states has a trivial dependence on the energy gap $|\Delta_{\mathcal{R}}|$, as can be seen from the spectral function associated with $\widetilde{G}^r_s(\varepsilon)$. When the single level moves away from the position of the chemical potential $\varepsilon_0 = 0.2|\Delta_{\mathcal{L}}|$ (Fig. 12(c)), or the coupling to the superconductors becomes asymmetric $\Gamma^{\mathcal{R}s} = 4\Gamma^{\mathcal{L}s}$ (Fig. 12(d)), the abrupt jump at $\varphi_s = \pi$ is smoothed out and the current-phase approaches the sinusoidal relation. The transmission probability becomes smaller when the level moves away from the chemical potential or the elastic couplings becomes asymmetric. As a result the link between these two superconductors becomes wicker, and thus the current-phase relation $\mathcal{I}(\varphi_s) \propto \sin\varphi_s$ is expected.[31] As the single level moves away from the chemical potential or the couplings become unequal, the DC Josephson current is significantly suppressed, with the component $\mathcal{I}_1$ from the discrete spectra suppressed while the component $\mathcal{I}_2$ from the continuum spectra $|\Delta_{\mathcal{L}}| < |\varepsilon| < |\Delta_{\mathcal{R}}|$ enhanced. The suppression of $\mathcal{I}_1$ is due to the decrease in the resonant Josephson tunneling probability which is originated from the violation of the constructive interference between the wave-functions of the Andreev levels, while the enhancement of $\mathcal{I}_2$ results from the fact that the Andreev levels are pushed towards the region $|\Delta_{\mathcal{L}}| < |\varepsilon| < |\Delta_{\mathcal{R}}|$ and thus the leaky probability is increased.

In summary, we have shown in this subsection that the DC Josephson current in an asymmetric-gap resonant $S/I/N/I/S$ structure with a single level is slightly enhanced in contrast to the symmetric-gap case. The current-phase relation is closely related to the position of the single level and the symmetry between the couplings to the two superconducting leads.

IV. CONCLUDING REMARKS

We have developed a unified theory of electronic transport in a general two-terminal hybrid nanosystem, in which each lead can be either a ferromagnet or a superconductor. Within the Keldysh NEGF formalism, the current is expressed in terms of the local properties of the central interacting region, $\mathbf{G}^{r,a,</>}$ and the equilibrium distribution functions of the leads $\mathbf{f}_\gamma$. The ferromagnetism and superconducting proximity are treated on the same footing, incorporated into the tunneling Hamiltonian and the self-energy matrices after introducing a four-dimensional Nambu-spinor space and performing appropriate Bogoliubov transformations. With the help of some unitary *rotation* and *phase* matrices, one can demonstrate analytically the gauge invariance of the general current formula (31), and simplify it to the Meri-Wingree forms for specific structures. For some quantities, such as the chemical potential, magnetization orientation and the superconducting order parameter phase, only their relative value appears explicitly in the expressions of current. Moreover, resonant tunneling, strong electron correlations (Coulomb blockade, Kondo resonance etc.), ferromagnetism and superconductivity proximity effect can be investigated in a unified transport theory without introduction of any ad hoc assumptions. In addition, the energy- and bias-voltage-dependence of the level-width functions and distribution functions enters into the current formula in a strict and natural manner, allowing us to explore the I-V characteristics in the large bias limit. However, the disadvantage of applying first the Bogoliubov transformation for the ferromagnetic lead Hamiltonian is that we can only obtain the expressions for the sum of the spin-up and spin-down current, while the information about the spin components of the current is lost.

Applying the current formulae to the simplest DBTS where the interactions are ignored some interesting transport properties are revealed if one takes into consideration the finite energy band structure of the ferromagnets. We have reported on the current flowing through a non-interacting zero-dimensional central region, thus the results obtained are qualitatively right for a $2D$ quantum well with the attached emitter and/or the collector being ferromagnetic. In addition, we did not consider the spin-flip process due to the interfacial scattering or the existence of paramagnetic impurities inside the barrier. It is known that the spin-flip process may reduce the magnitude of the tunnel magnetoresistance of a $F/I/F$ junction.[70] Also, we can expect that the Andreev current spectrum in $F/I/N/I/S$ structures will be modified to a great extent in the presence of the spin-flip process, since the Andreev reflection may be enhanced with the assistance of such process.

In $F-QD-F$, $F-QD-S$ or $S-QD-S$ systems, electron-electron interactions inside the QD are important and thus one should consider the many-body correlation effect. One example is the Kondo effect at low temperatures.[71] In such a circumstance, one has to calculate the full Green functions of the QD in the presence of electron-electron interactions, taking into consideration the couplings between the QD and the leads. We are aware of three recent preprints[72] on the Kondo physics in $F-QD-F$ systems in which the wide-band approximation is used.[16,72] Such a simplification of the ferromagnetic DOS may lead to even spurious results in $I-V$ characteristics. However. interesting and even unexpected Kondo resonances in these systems may arise with the full consideration of the finite energy band structure of the ferromagnetic leads.

Acknowledgments

Z. Y. Zeng and B. Li have been supported in part by the Academic Research Fund of the National University of Singapore and DSTA of Singapore. F. Claro has been supported by Cátedra Presidencial en Ciencias of Chile and FONDECYT 1020829 of Chile.

APPENDIX A: DERIVATION OF THE SELF-ENERGY MATRICES $\boldsymbol{\Sigma}^{r,a,</>}_{\gamma f/s}$

In this Appendix we derive various kinds of self-energy matrices for the elastic couplings between the central region and the ferromagnetic and superconductor leads.

First, we calculate the retarded/advanced self-energy matrix $\boldsymbol{\Sigma}^{r/a}_{\gamma f;nm}(t_1,t_2)$ arising from the coupling between the central normal metal and the ferromagnetic lead

$$\begin{aligned}\boldsymbol{\Sigma}^{r/a}_{\gamma f;nm}(t_1,t_2) &= \sum_k \mathbf{V}^{\gamma f\dagger}_{kn}(t_1)\mathbf{g}^{r/a}_{\gamma fk,\gamma fk}(t_1,t_2)\mathbf{V}^{\gamma f}_{km}(t_2)\\ &= \sum_k \mathbf{P}^{\dagger}(\mu_\gamma c t_1)\mathbf{V}^{\gamma f\dagger}_{kn}\mathbf{R}^{f\dagger}(\frac{\theta_{\gamma f}}{2})\\ &\quad \mathbf{g}^{r/a}_{\gamma f,\gamma f}(t_1,t_2)\mathbf{R}^{f}(\frac{\theta_{\gamma f}}{2})\mathbf{V}^{\gamma f}_{km}\mathbf{P}^{\dagger}(\mu_\gamma c t_2).\end{aligned}$$

The sum over momentum k can be converted to energy integration, i.e., $\sum\limits_k \rightarrow \int d\varepsilon_{k\sigma}\rho^{\gamma f}_{\sigma}(\varepsilon_{k\sigma})$. Neglecting the level shift term, we get

$$\begin{aligned}\boldsymbol{\Sigma}^{r/a}_{\gamma f;nm}(t_1,t_2) &= \mp\frac{i}{2}\int\frac{d\varepsilon}{2\pi}e^{-i\varepsilon(t_1-t_2)}\mathbf{P}^{\dagger}(\mu_\gamma c t_1)\\ &\quad \mathbf{R}^{f\dagger}(\frac{\theta_{\gamma f}}{2})\boldsymbol{\Gamma}^{\gamma f}_{nm}(\varepsilon)\mathbf{R}^{f}(\frac{\theta_{\gamma f}}{2})\mathbf{P}(\mu_\gamma c t_2)\\ &= \mp\frac{i}{2}\int\frac{d\varepsilon}{2\pi}e^{-i\varepsilon(t_1-t_2)}\mathbf{R}^{f\dagger}(\frac{\theta_{\gamma f}}{2})\\ &\quad \boldsymbol{\Gamma}^{\gamma f}_{nm}(\varepsilon\mp\mu_\gamma c)\mathbf{R}^{f}(\frac{\theta_{\gamma f}}{2}),\end{aligned} \tag{A1}$$

in which

$$\begin{aligned}&\boldsymbol{\Gamma}^{\gamma f}_{nm}(\varepsilon\mp c)\\ &= \begin{pmatrix}\Gamma^{\gamma f}_{nm;\uparrow}(\varepsilon-c) & 0 & 0 & 0\\ 0 & \Gamma^{\gamma f}_{nm;\downarrow}(\varepsilon+c) & 0 & 0\\ 0 & 0 & \Gamma^{\gamma f}_{nm;\downarrow}(\varepsilon-c) & 0\\ 0 & 0 & 0 & \Gamma^{\gamma f}_{nm;\uparrow}(\varepsilon+c)\end{pmatrix},\end{aligned} \tag{A2}$$

$$\boldsymbol{\Gamma}^{\gamma f}_{nm}(\varepsilon) = \boldsymbol{\Gamma}^{\gamma f}_{nm}(\varepsilon\mp 0), \tag{A3}$$

with

$$\Gamma^{\gamma f}_{nm;\sigma}(\varepsilon) = 2\pi\rho^{\gamma f}_{\sigma}(\varepsilon)V^{\gamma f*}_{kn}V^{\gamma f}_{km}.$$

Similarly, after transforming the momentum sum $\sum_k$ into an integral $\int d\varepsilon_k\rho^{\gamma s}_N(\varepsilon_k)$, where $\rho^{\gamma s}_N$ is the normal state of the superconductor, we obtain the self-energy matrix due to the coupling of the central region to the superconducting lead

$$\begin{aligned}\boldsymbol{\Sigma}^{r/a}_{\gamma s;nm}(t_1,t_2) &= \sum_k \mathbf{V}^{\gamma s\dagger}_{kn}(t_1)\mathbf{g}^{r/a}_{\gamma sk,\gamma sk}(t_1,t_2)\mathbf{V}^{\gamma s}_{km}(t_2)\\ &= \mp\frac{i}{2}\int\frac{d\varepsilon}{2\pi}e^{-i\varepsilon(t_1-t_2)/\hbar}\mathbf{P}^{\dagger}(\mu_\gamma c t_1+\frac{\varphi_\gamma}{2})\end{aligned}$$

$$
\begin{aligned}
&\mathbf{\Gamma}^{\gamma s}_{\varrho/\varrho^*;nm}(\varepsilon)\mathbf{P}(\mu_\gamma c t_2+\frac{\varphi_\gamma}{2}) \\
&= \mp\frac{i}{2}\int\frac{d\varepsilon}{2\pi}e^{-i\varepsilon(t_1-t_2)/\hbar}\mathbf{P}^\dagger(\mu_\gamma c t_1+\frac{\varphi_\gamma}{2}) \\
&\quad \mathbf{\Gamma}^{\gamma s}_{\varrho/\varrho^*;nm}(\varepsilon\mp\mu_\gamma c)\mathbf{P}(\mu_\gamma c t_1+\frac{\varphi_\gamma}{2}) \quad \text{(A4)}\\
&= \mp\frac{i}{2}\int\frac{d\varepsilon}{2\pi}e^{-i\varepsilon(t_1-t_2)/\hbar}\mathbf{P}^\dagger(\mu_\gamma c t_2+\frac{\varphi_\gamma}{2}) \\
&\quad [\mathbf{\Gamma}^{\gamma s}_{\varrho/\varrho^*;nm}]^T(\varepsilon\mp\mu_\gamma c)\mathbf{P}(\mu_\gamma c t_2+\frac{\varphi_\gamma}{2}), \quad \text{(A5)}
\end{aligned}
$$

where we have defined the complex level-width matrix as

$$
\begin{aligned}
\mathbf{\Gamma}^{\gamma s}_{\varrho;nm}(\varepsilon\mp c) &= \Gamma^{\gamma s}_{nm}
\begin{pmatrix}
\varrho^{\gamma s}(\varepsilon-c) & -\frac{|\Delta_\gamma|}{\varepsilon+c}\varrho^{\gamma s}(\varepsilon+c) & 0 & 0 \\
-\frac{|\Delta_\gamma|}{\varepsilon-c}\varrho^{\gamma s}(\varepsilon-c) & \varrho^{\gamma s}(\varepsilon+c) & 0 & 0 \\
0 & 0 & \varrho^{\gamma s}(\varepsilon-c) & \frac{|\Delta_\gamma|}{\varepsilon+c}\varrho^{\gamma s}(\varepsilon+c) \\
0 & 0 & \frac{|\Delta_\gamma|}{\varepsilon-c}\varrho^{\gamma s}(\varepsilon-c) & \varrho^{\gamma s}(\varepsilon+c)
\end{pmatrix}, \\
\mathbf{\Gamma}^{\gamma s}_{\varrho^*;nm}(\varepsilon\mp c) &= [\mathbf{\Gamma}^{\gamma s}_{\varrho;nm}(\varepsilon\mp c)]^*, \qquad \text{(A6)}
\end{aligned}
$$

with

$$
\begin{aligned}
\Gamma^{\gamma s}_{nm} &= 2\pi\rho^{\gamma s}_N(0)V^{\gamma s*}_{kn}V^{\gamma s}_{km}, \\
\varrho^{\gamma s}(\varepsilon) &= \frac{|\varepsilon|\vartheta(|\varepsilon|-|\Delta_\gamma|)}{\sqrt{\varepsilon^2-|\Delta_\gamma|^2}}-i\frac{\varepsilon\vartheta(|\Delta_\gamma|-|\varepsilon|)}{\sqrt{|\Delta_\gamma|^2-\varepsilon^2}}. \qquad \text{(A7)}
\end{aligned}
$$

Here we have defined a complex superconducting DOS, extending to the forbidden region in the usual BCS theory $|\varepsilon|<|\Delta_\gamma|$, inside which the Andreev reflection processes arise, as shown in the Blonder-Tinkham-Klapwijk theory.[55] When $|\varepsilon|<|\Delta_\gamma|$, the quasi-particle density of states ϱ is purely imaginary, indicating evanescent states in the gap which eventually decay into the pair condensate. The quasi-particle density of states of the superconducting lead γ is defined as

$$
\begin{aligned}
\rho^{\gamma s}(\varepsilon) &= \frac{1}{\pi}\mathrm{Im}\hat{g}^a_{\gamma s,\gamma s;11}=\frac{|\varepsilon|\vartheta(|\varepsilon|-|\Delta_\gamma|)}{\sqrt{\varepsilon^2-|\Delta_\gamma|^2}} \\
&= \mathrm{Re}\varrho(\varepsilon). \qquad \text{(A8)}
\end{aligned}
$$

In deriving Eq. (A4) we have used the following equalities

$$
\begin{aligned}
&\vartheta(\tau)\int_{-\infty}^{+\infty} d\epsilon_k \;\; [\cos^2\theta_{\gamma sk}e^{\pm i\sqrt{\varepsilon_k^2+|\Delta_\gamma|^2}\tau/\hbar}+ \\
&\qquad \sin^2\theta_{\gamma sk}e^{\mp i\sqrt{\epsilon_k^2+|\Delta_\gamma|^2}\tau/\hbar}] \\
&= i\int\frac{d\varepsilon}{2\pi}e^{-i\varepsilon\tau/\hbar}\int_{-\infty}^{+\infty}d\varepsilon_k\frac{\varepsilon\pm\varepsilon_k}{\varepsilon^2-\varepsilon_k^2-|\Delta_\gamma|^2} \\
&= \int d\varepsilon e^{-i\varepsilon\tau/\hbar}\varrho^{\gamma s}(\varepsilon), \\
&\vartheta(-\tau)\int_{-\infty}^{+\infty} d\epsilon_k \;\; [\cos^2\theta_{\gamma sk}e^{\pm i\sqrt{\varepsilon_k^2+|\Delta_\gamma|^2}\tau/\hbar}+ \\
&\qquad \sin^2\theta_{\gamma sk}e^{\mp i\sqrt{\epsilon_k^2+|\Delta_\gamma|^2}\tau/\hbar}] \\
&= -i\int\frac{d\varepsilon}{2\pi}e^{-i\varepsilon\tau/\hbar}\int_{-\infty}^{+\infty}d\varepsilon_k\frac{\varepsilon\pm\varepsilon_k}{\varepsilon^2-\varepsilon_k^2-|\Delta_\gamma|^2} \\
&= \int d\varepsilon e^{-i\varepsilon\tau/\hbar}[\varrho^{\gamma s}(\varepsilon)]^*, \\
&\vartheta(\tau)\int_{-\infty}^{+\infty} d\varepsilon_k \;\; \frac{\sin(2\theta_{\gamma sk})}{2}(e^{-i\sqrt{\varepsilon_k^2+|\Delta_\gamma|^2}\tau/\hbar}- \\
&\qquad e^{i\sqrt{\varepsilon_k^2+|\Delta_\gamma|^2}\tau/\hbar}) \\
&= i\int\frac{d\varepsilon}{2\pi}e^{-i\varepsilon\tau/\hbar}\int_{-\infty}^{+\infty}d\varepsilon_k\frac{|\Delta_\gamma|}{\varepsilon^2-\varepsilon_k^2-|\Delta_\gamma|^2} \\
&= \int d\varepsilon e^{-i\varepsilon\tau/\hbar}\varrho^{\gamma s}(\varepsilon)\frac{|\Delta_\gamma|}{\varepsilon}, \\
&\vartheta(-\tau)\int_{-\infty}^{+\infty} d\varepsilon_k \;\; \frac{\sin(2\theta_{\gamma sk})}{2}(e^{-i\sqrt{\varepsilon_k^2+|\Delta_\gamma|^2}\tau/\hbar}- \\
&\qquad e^{i\sqrt{\varepsilon_k^2+|\Delta_\gamma|^2}\tau/\hbar}) \\
&= -i\int\frac{d\varepsilon}{2\pi}e^{-i\varepsilon\tau/\hbar}\int_{-\infty}^{+\infty}d\varepsilon_k\frac{|\Delta_\gamma|}{\varepsilon^2-\varepsilon_k^2-|\Delta_\gamma|^2} \\
&= \int d\varepsilon e^{-i\varepsilon\tau/\hbar}[\varrho^{\gamma s}(\varepsilon)]^*\frac{|\Delta_\gamma|}{\varepsilon}.
\end{aligned}
$$

Note that we have chosen different complex half-planes in the contour integrations, in order to guarantee that the retarded/advanced self-energy matrices satisfy $\mathbf{\Sigma}^r_{\gamma s}(\varepsilon)=[\mathbf{\Sigma}^a_{\gamma s}(\varepsilon)]^\dagger$.

The lesser/greater self-energy matrix defined by

$$
\mathbf{\Sigma}^{</>}_{\gamma f/s;nm}(t_1,t_2)=\sum_k\mathbf{V}^{\gamma s/s\dagger}_{kn}(t_1)\mathbf{g}^{</>}_{\gamma f/s,\gamma f/s}(t_1,t_2)\mathbf{V}^{\gamma f/s}_{km}(t_2)
$$

are obtained in a similar way

$$
\begin{aligned}
\mathbf{\Sigma}^{</>}_{\gamma f;nm}(t_1,t_2) &= i\int\frac{d\varepsilon}{2\pi}e^{-i\varepsilon(t_1-t_2)/\hbar}\mathbf{P}^\dagger(\mu_\gamma c t_1)\mathbf{R}^{f\dagger}(\frac{\theta_{\gamma f}}{2}) \\
&\quad \mathbf{\Gamma}^{\gamma f}_{nm}(\varepsilon)\mathbf{R}^f(\frac{\theta_{\gamma f}}{2})[\mathbf{f}_\gamma(\varepsilon)-\frac{1}{2}\mathbf{1}\pm\frac{1}{2}\mathbf{1}]\mathbf{P}(\mu_\gamma c t_2) \\
&= i\int\frac{d\varepsilon}{2\pi}e^{-i\varepsilon(t_1-t_2)/\hbar}\mathbf{R}^{f\dagger}(\frac{\theta_{\gamma f}}{2}) \\
&\quad \mathbf{\Gamma}^{\gamma f}_{nm}(\varepsilon\mp\mu_\gamma c)\mathbf{R}^f(\frac{\theta_{\gamma f}}{2})[\mathbf{f}_\gamma(\varepsilon\mp\mu_\gamma c)-\frac{1}{2}\mathbf{1}\pm\frac{1}{2}\mathbf{1}], \qquad \text{(A9)}\\
\mathbf{\Sigma}^{</>}_{\gamma s;nm}(t_1,t_2) &= i\int\frac{d\varepsilon}{2\pi}e^{-i\varepsilon(t_1-t_2)/\hbar}\mathbf{P}^\dagger(\mu_\gamma c t_1+\frac{\varphi_\gamma}{2}) \\
&\quad \mathbf{\Gamma}^{\gamma s}_{\rho;nm}(\varepsilon)[\mathbf{f}_\gamma(\varepsilon)-\frac{1}{2}\mathbf{1}\pm\frac{1}{2}\mathbf{1}]\mathbf{P}(\mu_\gamma c t_2+\frac{\varphi_\gamma}{2}) \\
&= i\int\frac{d\varepsilon}{2\pi}e^{-i\varepsilon(t_1-t_2)/\hbar}\mathbf{P}^\dagger(\mu_\gamma c t_1+\frac{\varphi_\gamma}{2}) \\
&\quad \mathbf{\Gamma}^{\gamma s}_{\rho;nm}(\varepsilon\mp\mu_\gamma c)[\mathbf{f}_\gamma(\varepsilon\mp\mu_\gamma c)-\frac{1}{2}\mathbf{1}\pm\frac{1}{2}\mathbf{1}] \\
&\quad \mathbf{P}(\mu_\gamma c t_1+\frac{\varphi_\gamma}{2}) \\
&= i\int\frac{d\varepsilon}{2\pi}e^{-i\varepsilon(t_1-t_2)/\hbar}\mathbf{P}^\dagger(\mu_\gamma c t_2+\frac{\varphi_\gamma}{2}) \\
&\quad [\mathbf{f}_\gamma(\varepsilon\mp\mu_\gamma c)-\frac{1}{2}\mathbf{1}\pm\frac{1}{2}\mathbf{1}][\mathbf{\Gamma}^{\gamma s}_{\rho;nm}(\varepsilon\mp\mu_\gamma c)]^T
\end{aligned}
$$

$$\mathbf{P}(\mu_{\gamma}ct_2+\frac{\varphi_{\gamma}}{2}), \tag{A10}$$

where the real level-width matrix is defined as

$$\mathbf{\Gamma}^{\gamma s}_{\rho;nm}(\varepsilon\mp c) \;=\; \Gamma^{\gamma s}_{nm} \begin{pmatrix} \rho^{\gamma s}(\varepsilon-c) & -\frac{|\Delta_\gamma|}{\varepsilon+c}\rho^{\gamma s}(\varepsilon+c) & 0 & 0 \\ -\frac{|\Delta_\gamma|}{\varepsilon-c}\rho^{\gamma s}(\varepsilon-c) & \rho^{\gamma s}(\varepsilon+c) & 0 & 0 \\ 0 & 0 & \rho^{\gamma s}(\varepsilon-c) & \frac{|\Delta_\gamma|}{\varepsilon+c}\rho^{\gamma s}(\varepsilon+c) \\ 0 & 0 & \frac{|\Delta_\gamma|}{\varepsilon-c}\rho^{\gamma s}(\varepsilon-c) & \rho^{\gamma s}(\varepsilon+c) \end{pmatrix}.$$

The Fermi distribution matrix in the Numbu-spinor space takes the following form

$$\mathbf{f}_{\gamma}(\varepsilon\mp c) = \begin{pmatrix} f(\varepsilon-c) & 0 & 0 & 0 \\ 0 & f(\varepsilon+c) & 0 & 0 \\ 0 & 0 & f(\varepsilon-c) & 0 \\ 0 & 0 & 0 & f(\varepsilon+c) \end{pmatrix},$$

$$\mathbf{f}_{\gamma}(\varepsilon) = \mathbf{f}_{\gamma}(\varepsilon\mp 0). \tag{A11}$$

---

[1] For a review, see *Mesoscopic Electronic Transport*, Edited by L. L. Sohn, L. P. Kouwenhoven, and G. Schön, (Kluwer, Series E 345, 1997).

[2] C. Kittel, *Introduction to Solid State Physics* (Willy and Sons, New York, 1976).

[3] R. Kubo, M. Toda, and N. Hasnitsume, *Nonequilibrium Statistical Mechanics* (Springer-Verlag, Berlin, 1997).

[4] S. Datta, *Electronic Transport in Mesoscopic Systems* (Cambridge University Press, 1995), P246-273.

[5] R. Landauer, Philos. Mag. **21**, 863 (1970); M. Büttiker, Y. Imry, R. Landauer, and S. Pinhas, Phys. Rev. B **31**, 6207 (1985).

[6] L. P. Kadanoff and G. Baym, *Quantum Statistical Mechanics: Green Function Methods in Equilibrium and Nonequilibrium Problems* (Benjamin, New York, 1962).

[7] J. Rammer and H. Smith, Rev. Mod. Phys. **58**,323 (1986).

[8] G. D. Mahan, *Many-Particle Physics* (Kluwer Academic/Plenum Publishers, 2000).

[9] H. Haug and A. -P. Jauho, *Quantum Kinetics in Transport and Optics of Semiconductors* (Springer-Verlag, Berlin, 1998); D. Ferry, S. M. Goodnick, *Transport in Nanostructures* (Cambridge University Press, 1999).

[10] L. P. Keldysh, Sov. Phys. JETP **20**, 1018 (1965).

[11] C. Caroli, et al., J. Phys. C **4**, 917, 2598 (1971); **5**, 21 (1972); R. Combescot, ibid. **5**, 2611 (1971).

[12] Y. Meir and N. S. Wingreen, Phys. Rev. Lett. **68**, 2512 (1992); S. Hershfield, J. H. Davies and J. W. Wilkins, ibid. **67**, 3720 (1991); A. P. Jauho, N. S. Wingreen, and Y. Meir, Phys. Rev. B **50**, 5528 (1994).

[13] J. C. Cuevas, A. Martin-Rodero, and A. L. Yeyati, Phys. Rev. B **54**, 7366 (1996).

[14] R. Fazio and R. Raimondi, Phys. Rev. Lett. **80**, 2913 (1998); Superlatt.and Microstruc., **25**, 1141, 1999

[15] Q. F. Sun, J. Wang, and T. H. Lin, Phys. Rev. B **59**, 3831 (1999).

[16] B. G. Wang, J. Wang, and H. Guo, J. Phys. Soc. Jpn. **70**, 2645 (2001); N. Sergueev, Q. F. Sun, H. Guo, B. G. Wang, and J. Wang, Phys. Rev. B **65**, 165303 (2002).

[17] Y. Zhu, Q. F. Sun, T.H. Lin, Phys. Rev. B **65**, 024516 (2002).

[20] Yu. V. Nazarov, Phys. Rev. Lett. **73**, 1420 (1994); Superlatt. and Microstruc. **25**, 1221 (1999).

[19] N. B. Kopnin, *Theory of nonequilibrium superconductivity* (Oxford University Press, 2001).

[20] L. S. Levitov, H. Lee, and G. B. Lesovik, J. Math. Phys. **37**,4845 (1996); A. Brataas, Yu. V. Nazarov, and G. E. W. Bauer, Phys. Rev. Lett. **84**, 2481 (2000); Eur. Phys. J. B **62**, 5700 (2001); W. Belzig and Yu. V. Nazarov, Phys. Rev. Lett. **87**, 067006 (2001); ibid., 197006 (2001); Daniel Huertas-Hernando, Yu.V. Nazarov, and W. Belzig, ibid., **88**, 047003 (2002); cond-matt/0204116 (2002).

[21] For a reference, see Superlattices and Microstructures, **25**, No. 5/6, (1999).

[22] W. Poirier, D. Mailly, and M. Sanquer, Phys. Rev. Lett. **79**, 2105 (1997).

[23] S. K. Upadhyay, A. Palanisami, R. N. Louie, and R. A. Buhrman, Phys. Rev. Lett. **81**, 3247 (1999).

[24] A. F. Morpurgo, B. J. van Wees, T. M. Klapwijk, and G. Borghs, Phys. Rev. Lett. **79**, 4010 (1997).

[25] M. D. Lawrence and N. Giordano, J. Phys. Condens. Matter **39**, L563(1996).

[26] M. T. Tuominen, J. M. Hergenrother, T. S. Tighe, and M. Tinkham, Phys. Rev. Lett. **69**, 1997 (1992).

[27] T. M. Eiles, John M. Martinis, and Michel H. Devoret, Phys. Rev. Lett. **70**, 1862 (1993).

[28] S. Gueron, Mandar M. Deshmukh, E. B. Myers, and D. C. Ralph, Phys. Rev. Lett. **83**, 4148 (1999).

[29] A. F. Andreev, Sov. Phys. JETP **19**, 1228 (1964).

[30] For a reference, see Supplatt. and Microstruc. **25**, Issues 5-6 (1999).

[31] M. Tinkhma, *Introduction to Superconductivity* (Mcgraw-Hill, Inc 1996).

[32] I. O. Kulik, Sov. Phys. JETP **30**, 944 (1970).

[33] P. F. Bagwell, Phys. Rev. B **46**, 12573 (1992).

[34] G. A. Prinz, Science **282**, 1660 (1998).

[35] M. Julliere, Phys. Lett. A **54**, 225 (1975).

[36] M. J. M. de Jong and C. W. J. Beenakker, Phys. Rev. Lett. **74**, 1657 (1995).

[37] Z. Y. Zeng, Baowen Li, and F. Claro, Eur. Phys. J. B **32**, 401 (2003).

[38] J. C. Slonczewski, Phys. Rev. B **39**, 6995 (1989).

[39] D. Rogovin and D. J. Scalapino, Ann. Phys. **86**, 1 (1974).

[40] J. Bardeen, Phys. Rev. Lett. **9**, 147 (1962).

[41] D. C. Langreth, in *Linear and Nonlinear Transport in Solids*, Vol. 17 of *Nato Advanced Study Institute, Series B: Physics*, edited byJ. T. Devreese and V. E. Van Doren (Plenum, New York, 1976).

[42] G. B. Arnold, J. Low. Temp. Phys. **59**, 143 (1985).

[43] J. S. Moodera, et al., Phys. Rev. Let. **74**, 3273 (1995).

[44] D. E. Brehmer et al., Appl. Phys. Lett. **67**, 1268 (1995);

H. Ohno et al., ibid. **73**, 363 (1998).

[45] X. D. Zhang et al., Phys. Rev. B **56**, 5484 (1997).

[46] T. Tanamoto and S. Fujita, Phys. Rev. B **59**, 4985 (1999).

[47] L. Sheng et al., Phys. Rev. B **59**, 480 (1999).

[48] J. Barnas and A. Fert, Phys. Rev. Lett. **80**, 1058 (1998); S. Takahashi and S. Maekawa, ibid. **80**, 1758 (1998); S. Takahashi and S. Maekawa, ibig. **80**, 1758 91998); X. H. Wang and A. Brataas, ibid. **83**, 5138 (1999).

[49] A. G. Petukhov et al., Phys. Rev. Lett. **89**, 107205 (2002).

[50] M. B. Sterns, J. Magn. Mater. **5**, 167 (1977).

[51] A. M. Bratkovsky, Phys. Rev. B **56**, 2344 (1997).

[52] H. C. Liu and G. C. Aers, J. Appl. Phys. **65**,4908 (1989).

[53] G. Kim and G. B. Arnold, Phys. Rev. B **38**,3252 (1988).

[54] A. Brataas et al., Phys. Rev. B **59**, 93 (1999).

[55] G. E. Blonder, M. Tinkham, and T. M. Klapwijk, Phys. Rev. B **25**, 4515 (1982).

[56] C. W. J. Beenakker, Phys. Rev. B **46**,12841 (1992).

[57] N. R. Claughton, M. Leadbeater, and C. J. Lambert, J. Phys.: Condens. Matter **7**, 8757 (1995).

[58] A. L. Yeyati, J. C. Cuevas, A. L. Dvalos, and A. M.Rodero, Phys. Rev. B **55**, R6137 (1997).

[59] B. D. Josephson, Phys. Lett. **1**, 251 1962; Adv. Phys. **14**, 419 (1965).

[60] *Physics and Applications of Mesoscopic Josephson Junctions*, edited by H. Ohta and C. Ishii (The Physical Society of Japan, 1999).

[61] V. Ambegaokar and A. Baratoff, Phys. Rev. Lett. **10**, 486 (1963).

[62] P. G. de Gennes, *Superconductivity of Metals and Alloys* (W. A. Benjamin, New York, 1966).

[63] L.-F Chang and P. F. Bagwell, Phys. Rev. B **49**, 15853 (1994).

[64] L. I. Glazman and K. A. Matveev, JETP Lett. **49**, 659 (1989).

[65] S. Ishizaka, J. Sone, and T. Ando, Phys. Rev. B **52**, 8358 (1995).

[66] C. W. J. Beenakker, *Single-Electron Tunneling and Mesoscopic Devices* P 175-179, edited by H. Koch and H. Lübbig (Springer, Berlin, 1992).

[67] Q. F. Sun et al., Phys. Rev. B **61**, 4754 (2000); Y. Zhu et al., J. Phys.: Condens. Matter **13**, 8783 (2001); W. Li et al., condens-matt/0111480 (2001).

[68] C. W. J. Beenakker and H. van Houten, *Proc. Int. Symp. on Nanostructures and Mesoscopic Systems* P 481-497, edited by W. P. Kirk and M. A. Reed. (Academic Press, San Diego, 1992).

[69] B. J. van Wees, K. -M. H. Lenssen, and C. J. P. M. Harmans, Phys. Rev. B **44**, 470 (1991).

[70] X. D. Zhang, B. Z. Li, and F. C. Pu, Phys. Lett. A **236**, 356 (1997).

[71] L. I. Glazman and M. E. Raikh, JETP Lett. **47**, 452 (1988); Tai-Kai Ng and P. A. Lee, Phys. Rev. Lett. **61**, 1768 (1988).

[72] J. Martinek et al., cond-mat/0210006 (2002); P. Zhang et al., cond-mat/0210241 (2002); R. Lü et al., cond-mat/0210350 (2002).